2004-04-30

Performance of TOA Estimation Algorithms in Different Indoor Multipath Conditions

Nayef Ali Alsindi
Worcester Polytechnic Institute

Performance of TOA Estimation Algorithms in Different Indoor Multipath Conditions

A thesis submitted to the faculty of

Worcester Polytechnic Institute

in partial fulfillment of the requirements for the degree of

Masters of Science

in

Electrical and Computer Engineering

By

Nayef Ali Alsindi

April 2004

Prof. Kaveh Pahlavan, Thesis Advisor

Prof. Fred Looft, ECE Department Head, Thesis Committee

Prof. Wenjing Lou, Thesis Committee

To my parents

Abstract

Using Time of Arrival (TOA) as ranging metric is the most popular technique for accurate indoor positioning. Accuracy of measuring the distance using TOA is sensitive to the bandwidth of the system and the multipath condition between the wireless terminal and the access point.

In a telecommunication-specific application, the channel is divided into Line of Sight (LOS) and Obstructed Line of Sight (OLOS) based on the existence of physical obstruction between the transmitter and receiver. In indoor geolocation application, with extensive multipath conditions, the emphasis is placed on the behavior of the first path and the channel conditions are classified as Dominant Direct Path (DDP), Nondominant Direct Path (NDDP) and Undetected Direct Path (UDP). In general, as the bandwidth increases the distance measurement error decreases. However, for the so called UDP conditions the system exhibits substantially high distance measurement errors that can not be eliminated with the increase in the bandwidth of the system.

Based on existing measurements performed in CWINS, WPI a measurement database that contains adequate number of measurement samples of all the different classification is created. Comparative analysis of TOA estimation in different multipath conditions is carried out using the measurement database. The performance of super-resolution and traditional TOA estimation algorithms are then compared in LOS, OLOS DDP, NDDP and UDP conditions. Finally, the analysis of the effect of system bandwidth on the behavior of the TOA of the first path is presented.

Acknowledgments

I am greatly thankful to Professor Kaveh Pahlavan for his guidance in academics, research and general philosophy of life. My work and accomplishments were only possible because of his help and encouragement.

I am also very grateful to my fellow WPI friends, Bardia Alavi, Engin Ayturk, Mohammed Heidari for their continuous help and support. Their acquaintance has made my experience at WPI a remarkable one.

I am extremely grateful to members of the thesis committee, Professor Fred Looft and Professor Wenjing Lou.

I also take the opportunity to express my gratitude for the Fulbright Association and AMIDEAST for providing this valuable opportunity which funded my graduate studies.

Simply I could not have reached where I am today without my father, Dr. Ali Alsindi, my mother, Ms. Manar Fakhri, my brother Dr. Fahad Alsindi and my two sisters Noora and Muneera Alsindi. To them I dedicate this work and for them I continue to exist.

TABLE OF CONTENTS

LIST OF FIGURES

LIST OF TABLES

CHAPTER 1 Introduction

1.1 Background and Motivation

In recent years, a growing interest in location-finding systems have emerged for various geolocation applications. Two existing location finding systems, namely Global Positioning System (GPS) and wireless enhanced 911 (E-911), have been used to provide relatively accurate positioning for the outdoor environment [1]. These technologies, although accurate, could not provide the same accuracy when applied to indoor positioning. The different physical requirements of the indoor environment necessitate alternative systems to provide accurate positioning. Therefore, the design and development of indoor positioning systems requires in-depth modeling of the indoor wireless channel.

The importance of indoor geolocation can be apparent in different applications ranging from commercial to military [3]. Commercially, indoor geolocation could provide accurate and efficient positioning services for residential homes, where tracking children, the elderly or individuals with special needs, such as navigating the blind, could be of great importance. Locating specific items in stores and warehouses and locating in-demand equipment in hospitals are other examples of such services. In public safety applications indoor geolocation systems are needed to track inmates in prisons and navigate policeman and fire fighters through buildings and houses. On the military front, soldiers in urban warfare will use these applications to navigate inside buildings.

As a result of the potential for such application and services, the design and development of indoor positioning systems requires in-depth modeling of the indoor wireless channel. Radio propagation channel models are developed to provide a means to analyze the performance of a wireless receiver. Although many wideband radio models for telecommunication application exist in literature, their relevance to geolocation systems is distant [2]. In telecommunication application, the sought after parameters are the distance-power relationship and the multipath delay spread of the channel [3]. However, in geolocation application, the parameters of interest are the relative power and the time of arrival (TOA) of the direct line of sight (DLOS) path. Therefore, the accuracy of TOA measurement and modeling of the DLOS path is a measure of the performance of geolocation systems. However due to severe multipath conditions and the complexity of the radio propagation, the DLOS path cannot always be accurately detected [2, 4]. Improving the DLOS detection and TOA estimation requires enhancing the time domain resolution of the channel response in order to resolve the paths and enhance the accuracy of estimation.

Spectral estimation methods, namely super-resolution algorithms have been recently used by a number of researchers for time domain analysis of different applications. Specifically, they have been employed in frequency domain to estimate multipath time dispersion parameters such as mean excess delay and Root Mean Square (RMS) delay spread [5]. In addition, [6] used super-resolution algorithms to model indoor radio propagation channels with parametric harmonic signal models. Recently, however, super-resolution algorithms have been applied to accurate TOA estimation for indoor geolocation with diversity combining schemes [7]. The multiple signal classification

(MUSIC) algorithm was used as a super-resolution technique and it was shown to successfully improve the TOA estimation.

In indoor positioning, the behavior of TOA estimation in different environments is another important factor in determining the performance of geolocation systems. Besides the telecommunication-specific physical classification of line of sight (LOS) versus obstructed line of sight (OLOS), [2] have shown that there exists further classification that depends on the channel profile and the characteristics of the DLOS path. In the geolocation-specific classification, the first category is dominant direct path (DDP) where the DLOS path is detected and it is the strongest. The second category, nondominant direct path (NDDP) is when the DLOS path is detected but it is not the strongest. The last category is undetected direct path (UDP) where the DLOS is undetected.

In this thesis, a comprehensive measurement database has been created for these classifications with emphasis on finding more UDP cases. The performance and behavior of the DLOS distance error, which is directly related to TOA estimation error, is analyzed in all these different scenarios. In addition, the performance of different TOA estimation algorithms, namely, inverse Fourier transform (IFT), Direct Sequence Spread Spectrum (DSSS) and super-resolution Eigenvector (EV) algorithm is compared for different environments and bandwidths. The further classification of channel profiles and the performance analysis provide a deeper insight into wireless channel modeling for indoor geolocation.

1.2 Contribution of the Thesis

The contribution of the thesis can be summarized as follows. First, a method was devised for partitioning geolocation-based measurement database. Second, the existing measurement database was complemented for indoor positioning with additional measurements to develop a partitioned database of DDP, NDDP and UDP with adequate number of samples in each environment. Third, the statistical performance of TOA in different partitions or environments and different system bandwidths was evaluated using the comprehensive measurement database tailored to indoor geolocation. Finally, the effectiveness of super-resolution and traditional TOA estimation algorithms on the performance of indoor positioning system in different multipath environment was evaluated.

1.3 Outline of the Thesis

The rest of the thesis is outlined as follows. Chapter 2 provides an overview of indoor geolocation systems. The system architecture and geolocation specific matrices are explained. In addition a classification methodology is introduced for TOA-based indoor channel measurements. The importance of UDP condition on the behavior of the indoor channel is further examined. Chapter 3 outlines the procedure for the measurement campaign that was conducted along with detailed procedure for collecting the measurement samples. Also a UDP-specific measurement approach is described that shows the generation of more measurements with this condition. The creation of the measurement database is then described in further details. Chapter 4 introduces the different TOA estimation algorithms used in thesis. More specifically the IFT, DSSS and

the super-resolution EV/FBCM algorithms will be discussed. Chapter 5 provides the performance comparison in different indoor multipath environments. This includes comparing the performance of TOA estimation in different classification and indoor conditions and the analysis of different TOA estimation algorithms in those different environments. In addition the effect of the system bandwidth on the TOA estimation is also described. Finally Chapter 6 concludes the research results and discuss possibilities for future work.

CHAPTER 2 Background in Indoor Geolocation

Finding the accurate location of a user in an indoor environment has been recently both appealing and challenging to researchers. There is an emerging application for indoor geolocation that range from civilian to military. In certain applications the users can have an RF tag that can be worn and while walking through a building they can be located with accuracy. This could be implemented in schools where the young kids could be tagged so that the teacher knows exactly where they are at all times. In addition this technology can be used in hospitals to locate patients or in-demand equipment and medications. The harsh site-specific multipath environment introduces difficulties in accurately tracking the position of objects or people. The growing interest and demand for such applications dictates examining position more carefully. The indoor channel, as mentioned earlier, poses a serious challenge to system designers due to the harsh multipath environment. The behavior of the channel changes from building to the building and even within a single floor, the channel can change with added objects and people moving in the vicinity. As a result considerable work is needed for modeling the indoor channel for geolocation applications.

Section 2.1 will provide a brief overview of the different elements that make up a typical indoor geolocation system. In addition the different design approaches will be described with complementary examples. Section 2.2 will introduce the different indoor geolocation matrices that deal with different aspects of the physical layer. More specifically the TOA-geolocation based metric will be described in more detail since it is the focus of this thesis. Section 2.3 describes how the different indoor channel profiles

are partitioned and classified. Section 2.4 highlights the UDP problem and provides a more detailed description.

2.1 Elements of Indoor Geolocation

A typical functional block diagram of a wireless geolocation system is shown in Fig. 2.1. It is composed of three different blocks. The first is location sensing where the desired location metrics such as Angle of Arrival (AOA), Received Signal Strength (RSS) or TOA are extracted from the indoor propagation channel.

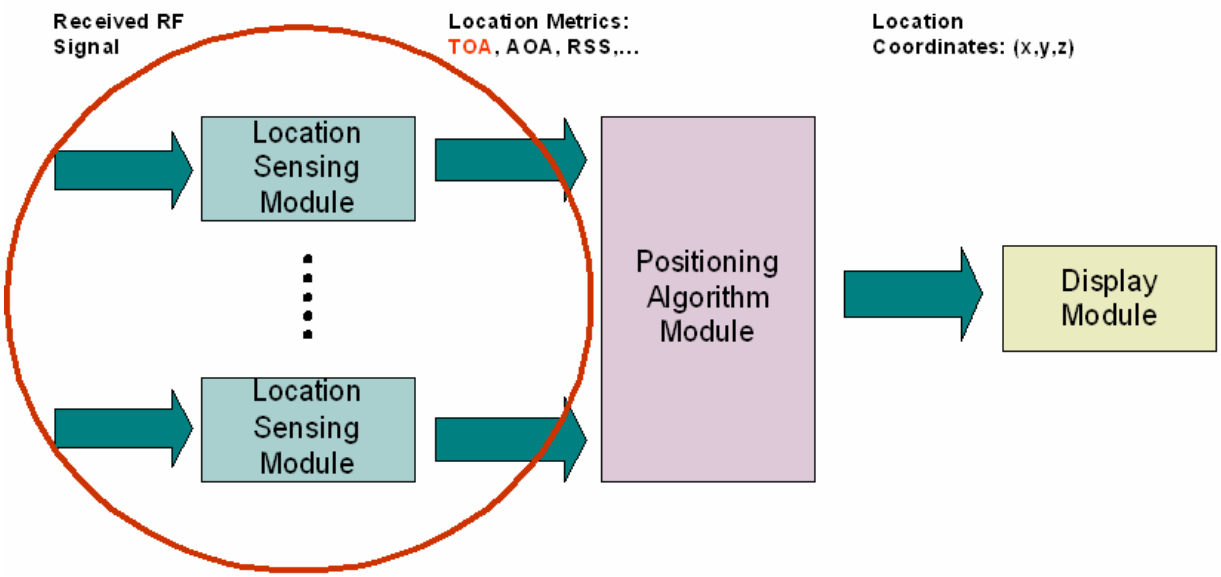

Figure 2.1: A functional block diagram of wireless geolocation systems.

Second, with a certain accuracy, these parameters are fed into the positioning algorithm block where it produces the (x, y, z) location co-ordinates. The algorithm receives the

measured metrics from the indoor channel with a certain error and tries to improve the positioning accuracy. As a result when the metric collection procedure lacks accuracy then the positioning algorithm will have to be more complex. For each metric a different technical foundation exists. This thesis focuses on TOA-based indoor geolocation. However it is worth mentioning the other metrics in order to have an overview of the different available positioning techniques. Finally the display system presents the location co-ordinates for the user. The system can provide the co-ordinates numerically or it can provide them in graphical user interfaces on a certain site-specific map. For example, the user can walk around with a PDA and can view his own location within a floor, or a worker tries to identify the location of a product in a warehouse, then he walks around with his display unit until he finds his desired object.

In general, there are two approaches for wireless indoor geolocation implementation. The first approach is to develop a signaling system and a network infrastructure of location sensors focused primarily on geolocation application [4]. The second is to use an existing wireless network infrastructure to locate a mobile terminal (MT) such as Wireless LAN (WLAN). The advantage of the first approach is that the system details are tailored towards the positioning application. The focus is on detecting the first path and all the system architecture building blocks are designed accordingly. In addition the overall design is under the control of the system designer. As a result the system could be implemented as small wearable tags or stickers and the complexity and density of the locating infrastructure can be customized according to the degree of accuracy needed. The second approach has the advantage that it avoids expensive and time-consuming infrastructure deployment. On the other hand, more intelligent

algorithms are needed in such systems to compensate for the low accuracy of the measured metrics.

In terms of system implementation when considering the first approach, the advantage is that the geolocation system is designed from the ground up. One way to approach it is the implementation of super-resolution algorithm for higher time-domain resolution. The system captures snapshots in the frequency domain and then through use of spectral estimation it is possible to obtain an accurate representation of the time-domain. In this thesis, this method is analyzed even further for different measurements conducted for indoor geolocation. Another emerging approach that has better accuracy and potential is Ultra wideband (UWB) technology. The large bandwidth provides high time-domain resolution which in return provides better ranging accuracy.

For the second approach, the use of the network infrastructure in indoor geolocation is also feasible but more complex algorithms are needed in order to compensate for overall design. One current example is Ekahau positioning software. Unlike the other positioning technologies, Ekahau does not apply propagation methods that suffer from multipath, scattering and attenuation effects. Instead Ekahau collects radio network sample points from different site location. Each sample point contains received signal intensity (RSSI) and the related map coordinates, stored in an area-specific positioning model for accurate tracking. Ekahau provides average positioning accuracy up to 1 meter. The software works with industry-standard Wi-Fi (IEEE 802.11b) networks [13]. When it comes to system deployment, a positioning model is created first. Then the positioning model is calibrated where RSSI samples are collected from the different points on the map. Then the tracking or positioning can start once the

system is calibrated. In other words, this positioning algorithms works with the WLAN infrastructure and no information about the access point locations is required. Such technology depends on complex positioning algorithms and does not concentrate on the physical layer. In fact, it uses RSS as a metric instead of trying to extract the TOA or AOA which is more challenging task at the physical layer. Needless to say, when following the RSS method and bypassing the propagation issues the complexities lie in the software itself.

2.2 Indoor Positioning Matrices

As mentioned earlier there are different metrics that can be used in indoor positioning. Although this thesis focuses on TOA-based indoor geolocation it is worth mentioning the other techniques. In AOA-based indoor geolocation direction-based triangulation is used, where two or more reference points (RP) are used to determine the position of the mobile terminal (MT). The AOA is usually measured with directional antennas or antenna arrays. This metric is not preferable in indoor environment because of the harsh multipath which introduces inaccuracies into the detection of the AOA in both LOS and OLOS conditions.

In RSS-based indoor geolocation, the received signal power can be easily measured at the receiver. The RSS is related to the distance between the transmitter and the receiver mathematically in the form of path loss models [3]. The path loss models portray the signal power attenuation as the signal travels through the indoor environment. If the path loss model is known in advance then the distance between the transmitter and receiver can be calculated by measuring the received signal strength and comparing to the

known path loss model. A wide variety of path loss models have been developed for different environments, each with different values of model parameters or different parameters and mathematical function forms [3]. The path loss model in indoor environment is highly site-specific. For example, the value of power-distance gradient, which is a parameter of path loss models, varies in a wide range between 15-20 dB/decade and a value as high as 70 dB/decade [3]. As a result of the complex indoor radio propagation channel, in practice the RSS-based indoor geolocation technique can be accomplished by estimating the path loss model of a specific indoor environment during system installation. In addition, there has to be a frequent re-estimation of the path loss model of the indoor radio propagation channel in order to establish accurate positioning values. An example of an RSS-based geolocation system is Ekahau software which was described earlier.

In TOA-based geolocation systems the important parameters are the TOA of the direct line of sight (DLOS) path since it is directly proportional to the physical distance between transmitting and receiving antennas. An example of the indoor multipath and the geolocation specific parameters is shown in Fig. 2.2. However since the system is not ideal – it has finite bandwidth, finite dynamic range, and introduces noise – the DLOS path can never be extracted perfectly from a measurement. The most reasonable approximation is the first detected path in the profile above a give noise floor. The other paths are also important since they can affect the TOA and amplitude of the first path [10]. The relative strength of the strongest path to the weakest path provides the dynamic range of the system and it is also important. The remaining paths are not very important

in geolocation. Instead they are more important for telecommunication in terms of multipath delay spread.

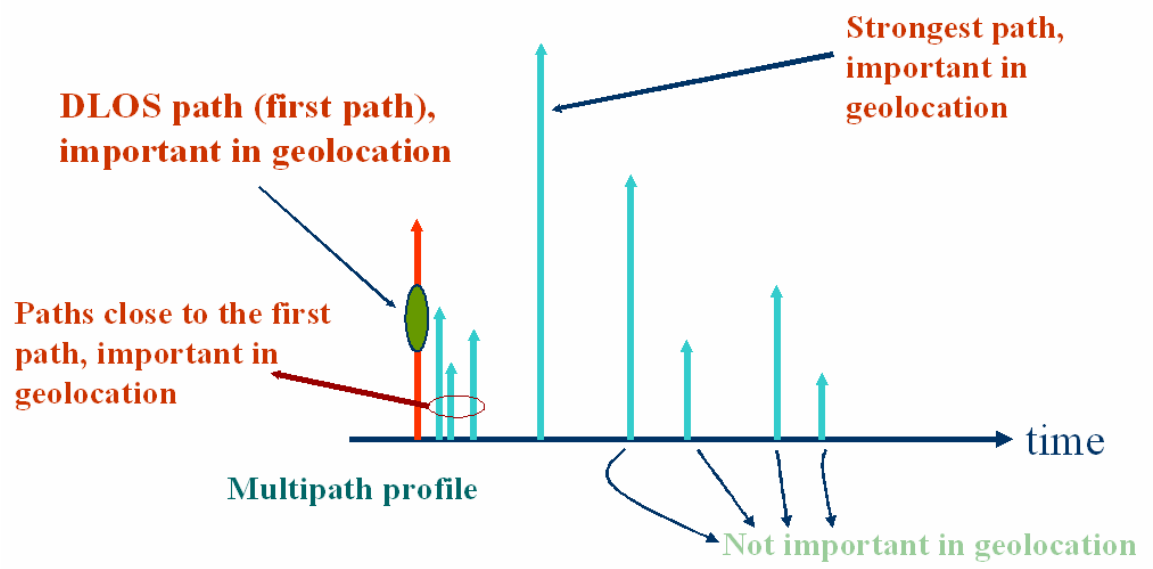

Figure 2.2: Multipath profile and important geolocation parameters.

Calculating the TOA from the channel profile requires several steps. To further clarify the procedure Fig. 2.3 shows a measured channel profile in the time-domain. For each measured profile calculating the TOA with exact accuracy is not possible due to multipath effects and finite bandwidths. However with a given expected TOA, there is an estimated TOA and thus a corresponding estimation error. This estimation error is directly related to the distance error through the speed of wave propagation, time and distance relationship.

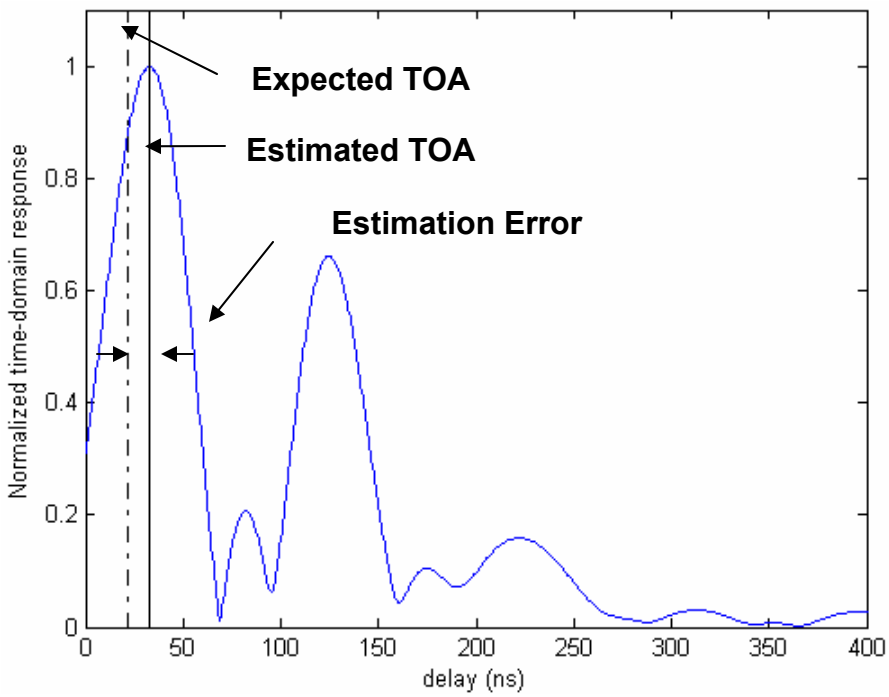

Figure 2.3: Normalized sample time-domain channel profile and TOA-based geolocation parameter calculations.

The objective of the estimation algorithms is to minimize this estimation error. In some cases this is achievable and in some others it is very difficult. A combination of system bandwidth and estimation algorithms can in fact reduce the error to acceptable levels, while at other cases this might not be achievable.

2.3 Partitioning of Indoor Geolocation Database

Wideband radio modeling for indoor geolocation application requires an in-depth characterization of the multipath behavior. Since the DLOS path is the most important parameter in indoor geolocation, the behavior of the channel profile or specifically the

TOA of the first path depends on the physical location of the receiver with regards to the transmitter. Thus it is pertinent to examine different measurement classifications to better analyze and characterize the behavior of TOA error. The performance of TOA estimation varies substantially in different environments. Two classification categories to be discussed next are based on the channel profile of the measurement data. Particularly, the first category is better suited for telecommunication modeling, since the behavior of root mean square (RMS) delay spread and distance-power relationship varies significantly between LOS and OLOS scenarios. The second classification is better suited for indoor geolocation modeling since it focuses on the behavior of the first path. In other words the measurement profile is categorized according to the power and availability of the DLOS path. The channel profiles were obtained by applying the IFT on the frequency domain measurement followed by a Hanning window.

2.3.1 Line of Sight and Obstructed Line of Sight

In wideband indoor radio propagation studies for telecommunication applications often channel profiles measured in different locations of a building are divided into line of sight and obstructed line of sight because the behavior of the channel in these two classes has substantially different impacts on the performance of a telecommunication system. When the transmitter and receiver have no physical obstructions between them the measurement is classified as LOS. When an obstruction exists, such as a wall, the profile is classified as OLOS. For instance in telecommunication applications the important channel characteristics are power distance relationship and multipath delay spread. The power distance relationship behaves differently in LOS as compared with

OLOS. The OLOS environment introduces larger power attenuation with distance. A similar situation holds for the multipath delay spread where OLOS introduce substantial number of multipath components when compared to LOS. This in turn reflects data rate limitations in indoor communications. However, this type of classification for the study of TOA indoor geolocation modeling has its limitations.

When considering this type of channel classifications for indoor geolocation different parameters are of concern namely, the TOA of the DLOS path and the relative power. As a result the desired channel classification should emphasize the behavior of the first path as opposed to the entire channel profile as desired in telecommunication applications. Grouping the channel profiles in LOS and OLOS for indoor geolocation does not provide a good insight into the behavior of the first path. For the former case, the DLOS path is the strongest and thus the TOA can be measured with great accuracy. In the latter, however, the DLOS path is obstructed by one to several walls depending on the location of the receiver. The accuracy of TOA in this case, suffers due to the unavailability of a strong DLOS path. In fact for some cases, the first path is undetectable causing the major error in the estimation of TOA. This classification lacks the ability to provide statistical analysis for the behavior of the first path. With OLOS the first path behavior ranges from the strongest to being undetected. When performing statistical analysis, OLOS does not provide an insight into the behavior of the DLOS path because it combines several multipath conditions together. A more insightful channel characterization is described in the next section where the emphasis is placed on classifying the different scenarios for the DLOS path.

2.3.2 DDP, NDDP and UDP

A more logical approach to categorizing the different channel profiles for indoor geolocation would be to consider the behavior of the DLOS path in each case.

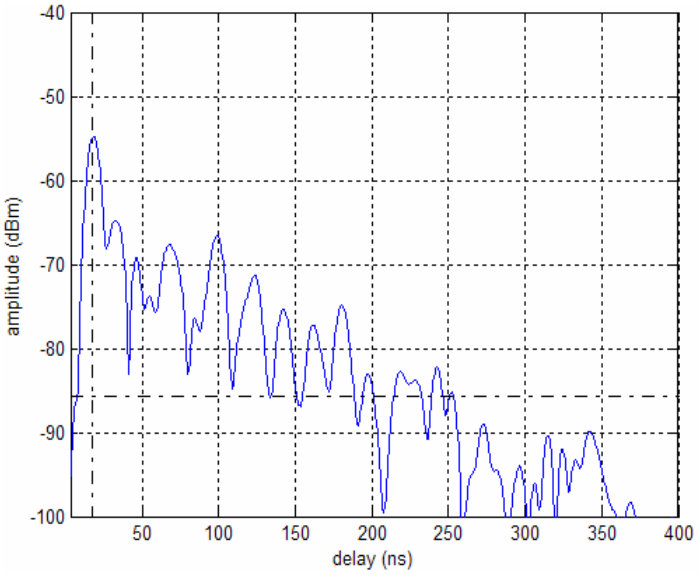

Figure 2.4: DDP measured channel profile obtained at 200 MHz bandwidth. Vertical dashed line is expected TOA and horizontal dashed line is the threshold.

Regardless of physical obstructions, the measurement is classified according to the availability and the strength of the DLOS path. The factors that affect categorizing the different profiles are receiver sensitivity and system dynamic range. These two constraints establish a threshold for use in characterization of the indoor multipath profiles. The receiver sensitivity is the noise level of the system where any path under that level cannot be a detected path. The dynamic range is defined as the ratio of the power of the strongest path to the power of the weakest detectable path in a measured

profile. For this categorization, a threshold was used in order to distinguish between a DDP, NDDP and a UDP. This threshold was selected based on the larger value of the measurement system noise floor (receiver sensitivity) and the side-lobes of the filtering window used (dynamic range). This ensured that the first peak of the channel profile is classified correctly. From these multipath conditions, DDP is the easiest to detect from the profile, as can be seen from Fig. 2.4 because it has a distinct strong first path. This category has an advantage where traditional GPS receivers can lock onto the DLOS path and detect its TOA accurately.

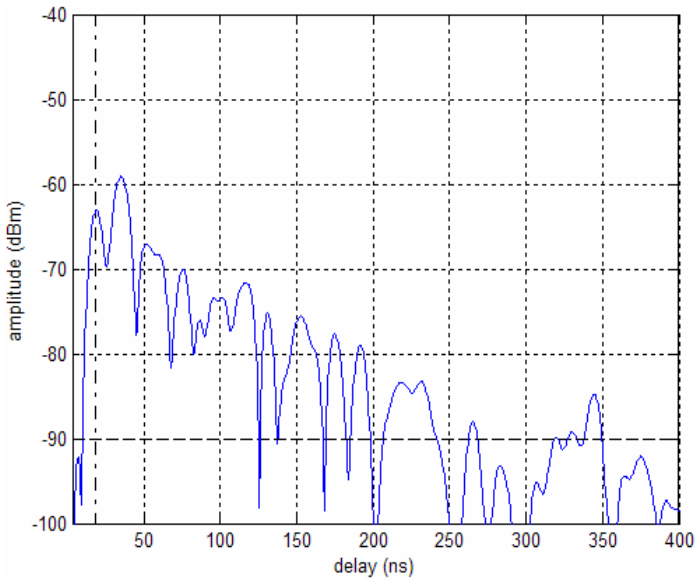

Figure 2.5: NDDP measured channel profile obtained at 200 MHz bandwidth. Vertical dashed line is expected TOA and horizontal dashed line is the threshold.

When the first path gets weaker but still above the threshold, the profile fits in the NDDP category which is shown in Fig. 2.5. For this case, a significant loss of accuracy in

TOA estimation can be reduced when a more complex RAKE receiver is used in order to resolve the multipath and intelligently detect the TOA of the DLOS path.

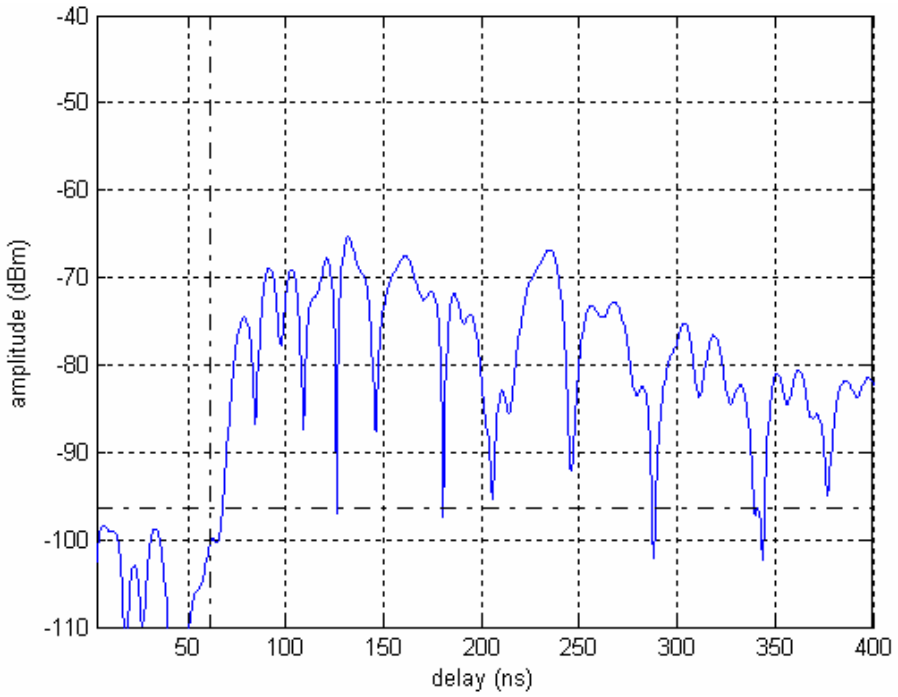

Figure 2.6: Measured UDP channel profile at 200 MHz. Vertical dashed line is expected TOA and horizontal dashed line is the threshold.

A profile is a UDP, when the first path is below the threshold indicating loss of the DLOS path as evident from Fig. 2.6. In this unfavorable situation neither the GPS nor the RAKE receiver can accurately detect the TOA and this, specifically, causes the most significant error in indoor positioning applications. If practical considerations regarding the dynamic range of the system are neglected then there are essentially two categories: DDP and NDDP. However, in reality, the implemented receiver will have limitation such as

sensitivity and dynamic range and this will create situations where the DLOS path cannot be detected.

Overall UDP is expected to show substantial degradation in TOA estimation for geolocation application when compared with the other scenarios. As a result it is important to understand how and why UDP situations arise in indoor environments. The next sections attempt to shed some light on this rather important case where a measurement campaign was set up to better analyze and understand this situations.

2.4 The Importance of UDP Condition on the Behavior of the Channel

The accuracy of TOA estimation in indoor geolocation application is the most important issue in distance estimation. The harsh indoor multipath conditions introduce a random dimension to the problem. The behavior of the first path changes in different locations depending on the indoor physical structure of the building and the channel characteristics. With these different channel classes described in the introduction, a major error contributor, UDP is the most significant obstacle to the accuracy of indoor geolocation systems.

A sample measured channel profile which describes the characteristics of the UDP case is shown in Fig. 2.6. It is clear that the non-DLOS paths have significant power when compared to the first path. This relative power drop is beyond the dynamic range of the measurement system. In most cases, UDP is caused by the existence of a metallic obstruction in the direct path. In other instances, there might be a number of walls that attenuate the first path considerably compared to the other paths. In both cases, the paths

arriving from other directions are much stronger. As a result when analyzing the performance of an indoor geolocation system it is important to have an in-depth evaluation on why and where this UDP occurs so that it can shed more light on how to avoid it.

However, in situations where UDP is unavoidable, the next step is to find ways to resolve it or reduce its effect on TOA estimation. One way is to use estimation algorithms to try to resolve the multipath and perhaps reduce the error in UDP conditions. A second approach might consider the bandwidth of the system. In many cases, when the bandwidth of the system increases, the time-domain resolution and thus the accuracy of TOA estimation increase. So could increasing the bandwidth actually solve this grave problem? Both the use of estimation algorithms and the system bandwidth will be discussed later and its effect on TOA estimation error will be analyzed.

In order to analyze the effect of TOA estimation errors in UDP conditions it is necessary to have an experimental basis to draw useful conclusions. As will be described in the next chapter, a measurement database was created for use in analysis. The special case of UDP did not receive a lot of attention in the past and the previous measurements were classified according to LOS and OLOS. As a result a measurement campaign was created to collect more UDP measurements for statistical analysis. Before that, however, a description of the measurement system and the database used in the analysis will provide both a clarification and justification for the measurement approach.

CHAPTER 3 Measurement Campaign and Database Partitioning

In the previous chapters, it was illustrated that the undesirable UDP condition introduces substantial ranging errors and can be a limiting factor in deployed geolocation systems. Analyzing the performance of indoor geolocation systems in this critical multipath condition requires an experimental basis on which to draw useful conclusions. Experimental measurements provide further insight and understanding into the causes of such a phenomenon and an evaluation of how severe the problem can be. By observing the statistical data that can be extracted from the measurements one could find out how much ranging error does UDP actually introduce compared to other multipath conditions such as DDP and NDDP. In addition, when comparing different TOA estimation algorithm it will be very helpful to have an experimental set of measurement data to analyze their performance in different multipath conditions. Furthermore these measurements could shed some light on how to avoid or mitigate this unfavorable condition. Previously, there were some indoor channel measurements reported in literature that were conducted by the Center for Wireless Information Networks (CWINS) laboratory at Worcester Polytechnic Institute (WPI) [9, 10]. These measurement campaigns, however, did not focus on the UDP problem and as a result lacked sufficient number of measurement points. They were mainly LOS and OLOS measurement scenarios in different buildings. The OLOS measurements had some UDP measurement points but they were not adequate. As a result, the lack of sufficient

measurements geared towards the UDP condition provided an incentive to start a measurement campaign and to create a database for statistical analysis.

The measurement campaign which will be discussed in details in this chapter is an effort to find locations where the probability of UDP occurrence is the greatest in order to collect more data samples. The measurement campaign is composed of two experimental setups. The first one, Setup 1, is a deterministic approach in terms of finding UDP conditions. The transmitter and receiver antennas were placed in locations that were expected in advance to introduce major attenuation to the first path and thus exhibit UDP symptoms. The second experiment, Setup 2, is more of a random approach where OLOS measurements were collected without a previous knowledge of the whereabouts of those conditions. This experimental campaign helped in the creation of a database that provided foundations for statistical analysis. The database is composed of this measurement campaign along with the other previous CWINS measurements. In this chapter, first the measurement system is described and then the procedure for finding and measuring UDP is explained. Finally the procedure for creating the database is outlined.

Section 3.1 provides a detailed description of the measurement system used to collect the data samples. Section 3.2 outlines the different steps taken to search for more UDP measurement samples used later for statistical analysis. Section 3.3 presents the measurement database and how it was put together.

3.1 Measurement System

One of the most popular techniques to experimentally calculate the TOA is through the use of a frequency domain measurement system which is described in [8]. The main component of the measurement system used is an HP-8753B network analyzer. Figure 3.1 shows the measurement system and its components.

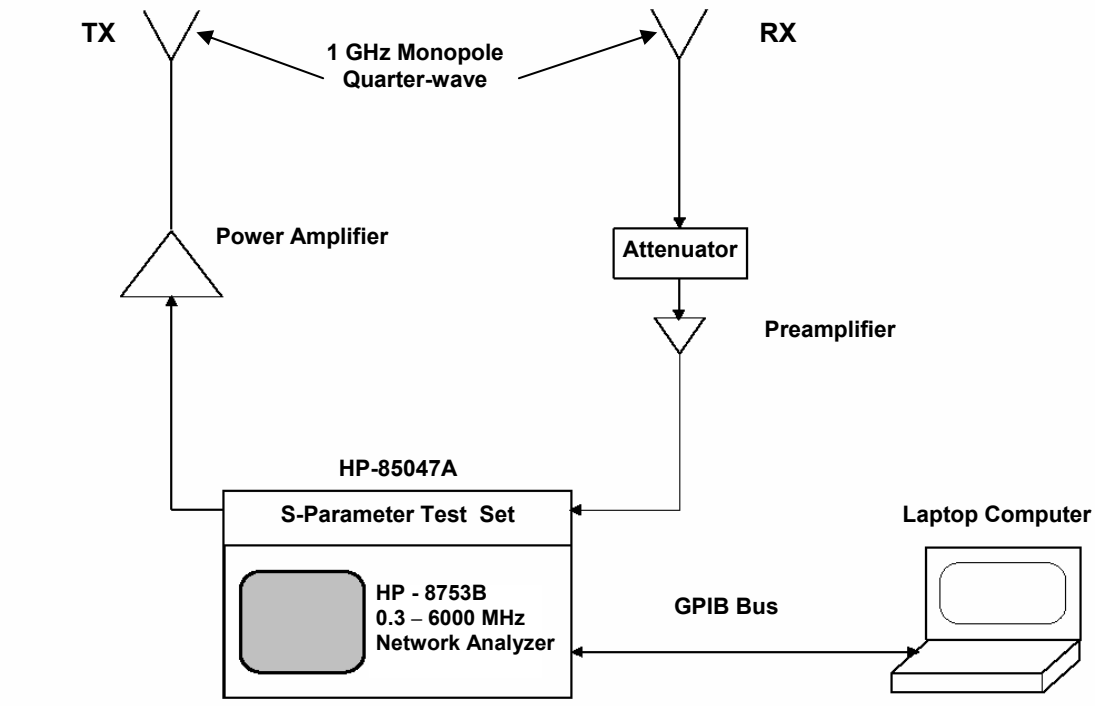

Figure 3.1: Frequency domain measurement system

The measurement system is composed of the network analyzer, a power amplifier, an attenuator and a pre-amplifier. The network analyzer is controlled by a laptop through a Hewlett Packard's version of a general-purpose instrumentation bus (GPIB) where a program is used to select the desired parameters of the measurement scenario. The laptop

initializes the network analyzer preceding each measurement where the start and stop sweeping frequencies are selected along with the number of desired samples and collects the data at the completion of each measurement. The transmitted signal passes through a 30 dB amplifier before going to the channel. The receiver component attenuates and pre-amplifies the incoming signal before passing it to the network analyzer. In this campaign, the network analyzer was used to sweep the frequency domain channel from 900 to 1100 MHz with 400 samples. The magnitude and phase of the measured frequency response were stored for each measurement and later used for further processing. Both the antennas used in the measurement system are 1 GHz monopole quarter wave adjusted on square plates.

Figure 3.2: 1 GHz monopole quarter wave antennas

Figure 3.2 shows a picture of the monopole quarter wave antennas. The dimension of the monopole corresponds to λ/4, where λ is the wavelength of the signal. The side of the ground plane corresponds to λ/2. The frequency domain measurements were conducted by fixing the transmit antenna and moving the receiver around the desired locations. After data collection, the measured frequency domain channel profiles were further processed and the time-domain channel profile was obtained by use of inverse Fourier transform (IFT). Since the noise floor of the measurement system is -100 dBm, and the Hanning window has side lobes of -31 dB below the maximum peak of the profile, a threshold is selected according to the larger value of the two. As mentioned earlier, this threshold is used to characterize the channel profile according to the power of the DLOS path.

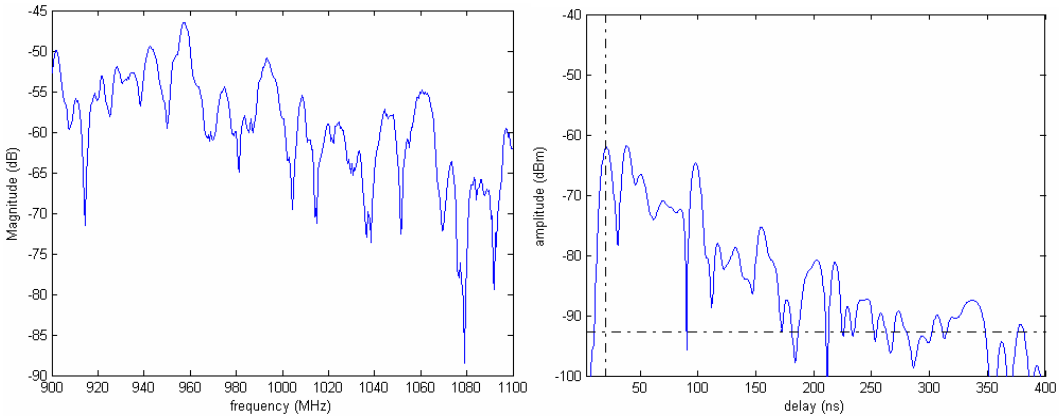

(a) (b)

Figure 3.3: (a) Sample frequency domain measurement (b) corresponding time-domain profile.

Figure 3.3 shows a sample frequency domain measurement and its corresponding time-domain profile. Notice the frequency selective fading in the frequency domain. Also the time-domain profile illustrates the multipath components arriving at different delays with the first path not the strongest which in this case it is an NDDP condition. In this figure, the time domain profile is obtained by application of the IFT followed by a Hanning window. In the next chapters different estimation algorithms will be introduced and it will be shown how they provide different resolution capabilities and thus different TOA estimation.

3.2 The Search for UDP

A simple yet insightful method to better understand UDP is to analyze the locations that maximize attenuation on the DLOS path in indoor environments. This provides a methodology to understand how and when UDP occurs. The measurement campaign is built on two measurement setups that deal with the occurrence of UDP differently. In Setup 1, a deterministic approach is followed where the selected receiver measurement points were expected to exhibit UDP characteristics because of the physical geometry and the actual obstruction in the DLOS path. In Setup 2 a more random approach is followed as several measurement points were taken but their nature was not expected in advance. In other words in the former approach, a prior examination of the floor plan showed that if the transmitter and receiver were placed in such locations, there is a high probability that the location exhibits a UDP condition. On the other hand, in the latter case it was not known beforehand what it would exactly produce.

The measurements were conducted in the Atwater Kent (AK) building, the Electrical and Computer Engineering (ECE) Department at WPI. The AK building was built in 1906 and had two major remodelings and additions in 1934 and 1981. Therefore, in some areas within the building there is more than one exterior-type wall. The exterior walls of this building are heavy brick, the interior walls are made of aluminum stud and sheet rock, the floors are made with metallic beams, the doors and windows are metallic, and many other metallic objects are spread over different laboratory areas. The excessive number of metallic objects and heavy and multiple external walls makes this building a very harsh environment for radio propagation. As a result this makes it a suitable building for indoor geolocation measurements since the DLOS path will be attenuated harshly in most cases. The measurement campaign was conducted on the third floor of AK building. The first step of the campaign procedure focused on the selection of the measurement points' locations. After careful examination of the 3rd floor plan, the location of the transmitter and receiver were selected to investigate the effect of walls and metallic objects on the DLOS path. As a result two different experimental setups were devised to provide different attenuation effects on the first path. Each setup involved placing the transmitter in a fixed location and moving the receiver around it through the corridors. As will be described later in more details, in the first setup the transmitter was located in AK 320, the CWINS laboratory, with the receiver points located around it in the corridors. In the second setup the transmitter was located in the corridor to the right of the CWINS laboratory while the receiver was moved through the corridors. Once the locations were determined, the measurement points were marked on the 3rd floor and the measurement campaign started. The measurements involved moving the receiver along the designated

points, measuring and recording the channel and proceeding to the next point. The saved measurement files were then used for further processing and analysis.

Setup 1 took advantage of a metallic chamber, better known as Faraday Chamber, residing in the CWINS lab. The transmitter was placed inside the lab and the receiver was moved around it through the corridors. Figure 3.4 shows the 3rd floor plan of AK building along with the location of the transmitter and receiver points for Setup 1. The metallic chamber designated by a gray box is situated in the corner of the lab. The receiver points shown in the figure were taken 1 meter apart. This helped to provide gradual snapshots into the channel profile as the receiver moves from one point to the next.

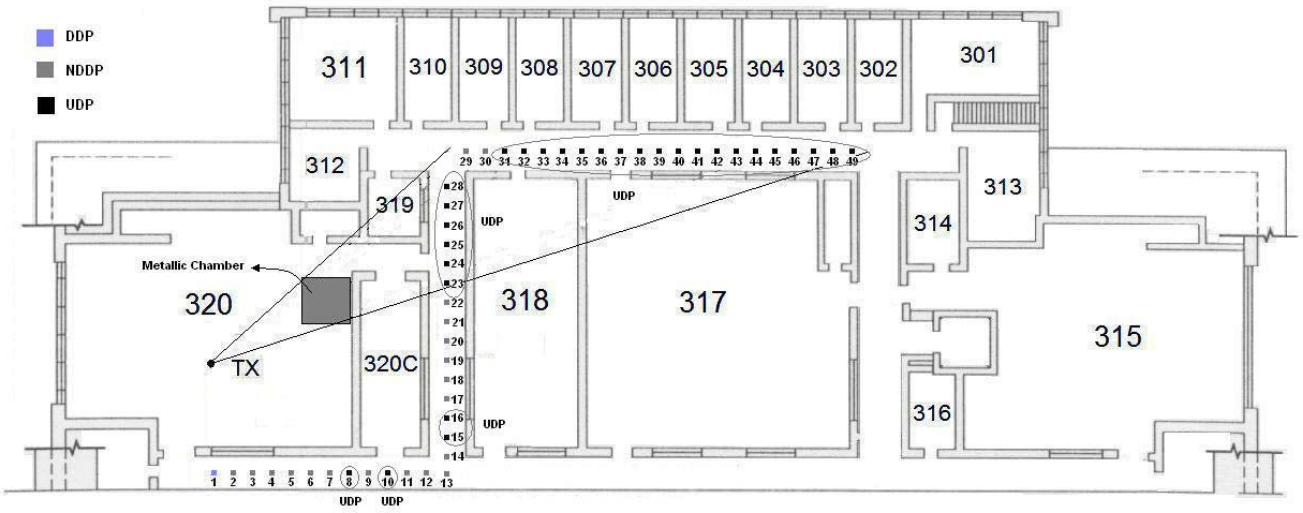

Figure 3.4: Measurement Setup 1 in AK building ECE department at WPI.

In other words, prior to conducting the measurements it was desirable to see what happens to the DLOS path as the receiver moves in a straight line from one point to the other. What would the first measurement point be? Would the measured channel profiles

change from DDP to NDDP gradually and eventually end up as UDP as the power of the first path weakens? Or would UDP conditions appear randomly between NDDP points? The answer to these questions would provide an insight into how the first path behaves and the nature of UDP occurrence. In radio propagation it is well known that metallic objects reflect most of the propagating wave and weaken the transmitted part. As a result it would be interesting to see whether the metallic chamber would produce UDP conditions or not.

The expectations for this part of the measurement campaign were as follows. The occurrence of UDP would be localized to the region shadowed by the metallic chamber as shown in Figure 3.4. It was, therefore, expected to exhibit UDP characteristics with high probability since the DLOS path suffers severe attenuation while the other paths arrive with relatively stronger power. In addition it was expected that the other measurement points not covered by the UDP region would most likely exhibit NDDP characteristics since they do not have a metallic chamber in their DLOS path.

After conducting the measurements and analyzing their channel characteristics, the outcome is interesting. In Figure 3.4 the light dots represent NDDP measurements points while the dark ones represent UDP. As expected the region shadowed by the chamber exhibited UDP characteristics. The DLOS path for those points was expected to experience severe attenuation. Indeed after analyzing the measurement data it was possible to see that the bounded region had a high probability of UDP occurrence. There are two points, however, in this region that appeared as NDDP. A possible explanation for this could be that since these two points are located exactly around the corner of the corridor, the diffracted path is very close to the direct path and this might have appeared

to be a stronger first path than expected. As for the other points in this region, it is clear that the chamber is the major factor in attenuating the first path. Another interesting observation is that in addition to the region affected by the chamber, there are four UDP points that occurred, namely points 8, 10, 15 and 16, in the corridor around the CWINS lab. This is a clear indication that this unfavorable condition occurs in different locations because of metallic objects or other obstructions that are not accounted for. In addition there was one DDP point, namely point 1, which is closest to the transmitter. Although the wall is an obstruction and this measurement point would be classified as OLOS, but the strong first path classifies it as DDP. The other NDDP points close to it have a strong first path, but they have other paths that are slightly stronger. The distance between the transmitter and receiver is directly related to the TOA and obtaining the distance from the TOA is simply the relationship with the speed of light. The estimated distance is obtained from the estimated TOA. As mentioned earlier, the frequency domain is converted to time-domain by application of the IFT. The results presented in this chapter all use the IFT with peak detection as the estimation algorithm. Later on, more complex TOA estimation algorithms will be introduced and their time-domain resolution and thus accuracy will vary. The distance error of UDP is substantially larger than NDDP or DDP. The distance error for UDP ranges from 3.7 to 10.8 meters. On the other hand, NDDP has a much lower error range, namely from 0.123 to 8.8 meters. Another interesting observation is that from this particular measurement setup 60% of the points are UDP condition and the majority of those were the outcome of the metallic chamber. Thus the prior expectations were valid with some interesting observations regarding the appearance of UDP in other locations.

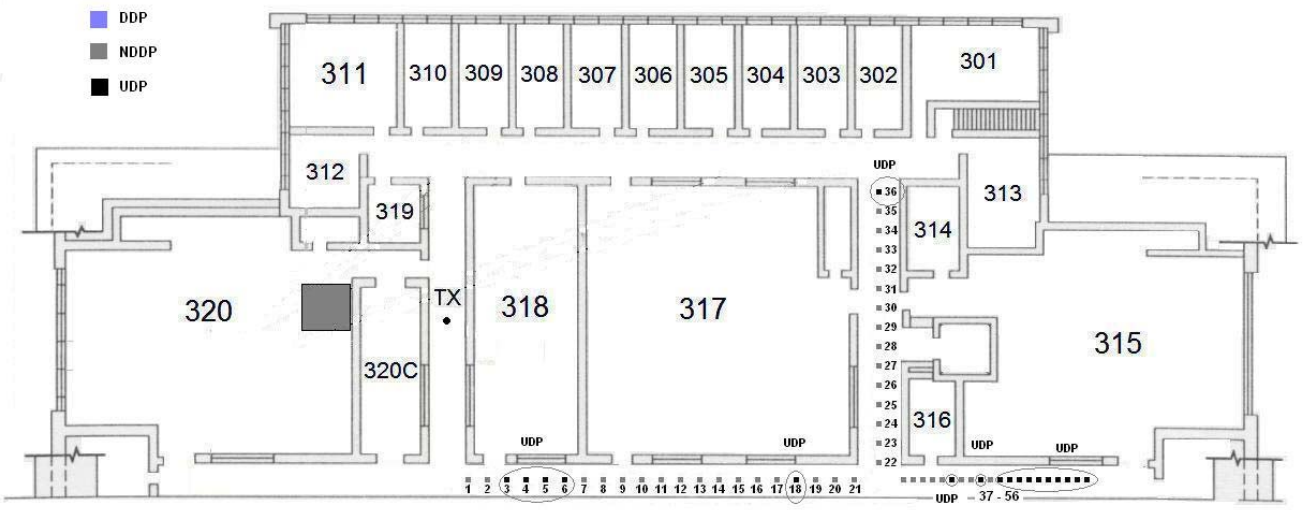

Figure 3.5: Setup 2 of the measurement campaign at 3rd floor of AK, the ECE department at WPI.

Setup 2 was conducted on the third floor of AK, and it focused on an ad hoc approach in measurements. The transmitter was fixed in the center of the corridor to the right of the CWINS lab as shown in Figure 3.5 and the receiver was moved in several points along the lower and parallel corridors. All the receiver points were 1 meter apart, except for the measurement points 37-56 they were 50 cm apart. On the contrary to the earlier experimental setup, the outcome of this approach was not known in advance and in addition fewer UDP points were expected and more of NDDP. However after analysis a substantial amount of UDP points, around 32% of the measurements which corresponds to 18 UDP points, were measured at different locations. Although this number is less than the previous setup, nonetheless, some interesting observations are introduced. It is

interesting to note how these unfavorable scenarios are not localized only to a certain region or corner of the floor plan, but rather they exist in "spots" strengthening the notion that the DLOS path can be lost in locations where system designers might have not predicted because of additional obstacles apart from the walls. In some cases UDP occurs between NDDP points and in others it occurs subsequently one after the other. For the former case this is mainly because of shadow fading caused by obstacles, in addition to walls, that suddenly attenuate the first path significantly. However for the latter case, the walls are the main contribution to the loss of the first path. The contribution of the walls can be supported by the results of measurement points 45-56 which are further highlighted in Fig. 3.5. The loss of DLOS path is a clear indication that the walls are the major factor attenuating its power since they are subsequently followed by each other. On the other hand UDP occurs in other locations where the walls are not the primary factor. For example, points 3-6 in Fig. 3.5 are UDP. There are two walls in the DLOS path of those points. However the number of walls for the other points such as 14, 15 or even 16 are greater but still they have a strong first path. For instance, points 22-35 are all NDDP and there are 3 to 4 walls in the DLOS path. In addition the distance is larger indicating further attenuation compared to points 3-6. The loss of the first path for points 3-6 is a clear indication of shadow fading caused by a metallic object such as a cabinet or shelf that might be located somewhere in room AK 318. Similar reasoning holds for UDP points 18 and 36 where the points before them and after them exhibit NDDP characteristics.

The estimated distance error as a result of this measurement campaign ranges from less than 1 meter to more than 10 meters in some cases. Figure 3.6 shows the scatter

plot of the distance error for setup 1 with the respective distance of the measurement campaign at 20 MHz system bandwidth.

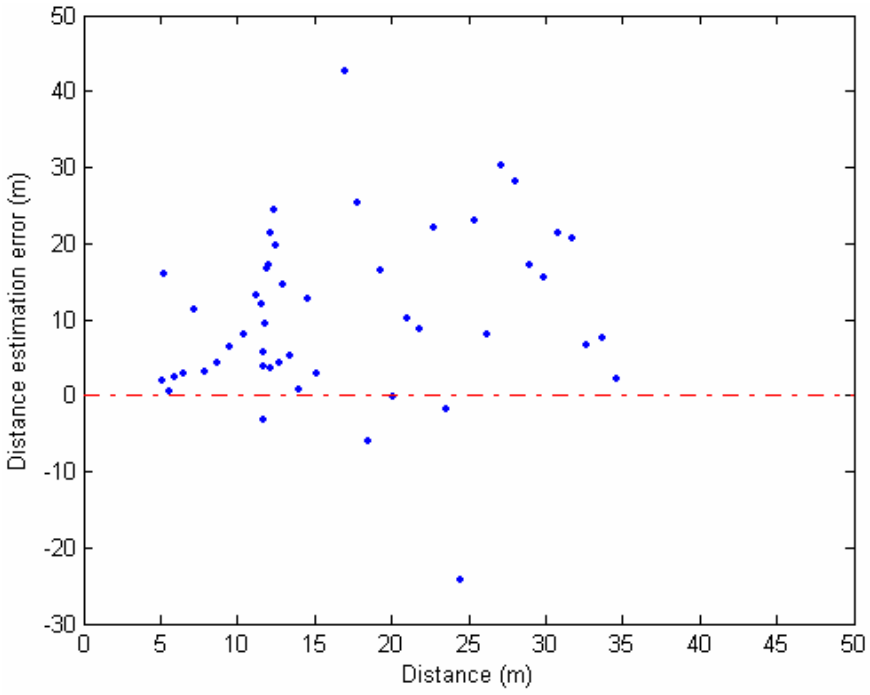

Figure 3.6: Scatter plot of the distance error for Setup 1 at 20 MHz bandwidth.

When the system bandwidth is further increased to 200 MHz the distance error decreases because of higher time-domain resolution. However still some of the measurement points, especially the UDP ones will continue to exhibit higher distance error. Figure 3.7 shows the scatter plot of the distance error for the same setup at 200 MHz bandwidth.

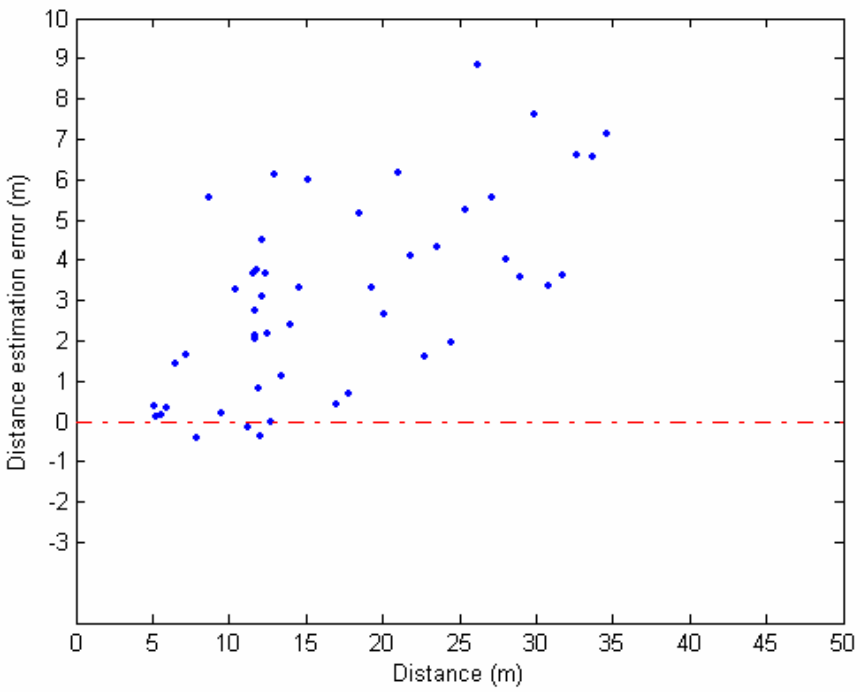

Figure 3.7: Scatter plot of the distance error for Setup 1 at 200 MHz bandwidth.

First, comparing Fig. 3.7 to Fig. 3.6 it is clear that the distance error drops significantly at the higher bandwidth. In fact the error drops well below 10 meters as compared to 40 m. Second, even at this higher bandwidth there are many measurement points exhibiting errors higher than 2 meters which is not acceptable for indoor geolocation. The majority of the error is contributed by UDP conditions. The outcome of Setup 2 is also worth observing in terms of distance error behavior. Figures 3.8 and 3.9 show the scatter plots of the distance error for Setup 2 at 20 and 200 MHz respectively. Again what is noticeable here is both the effect of increase in system bandwidth and the error values attributed to NDDP and UDP conditions.

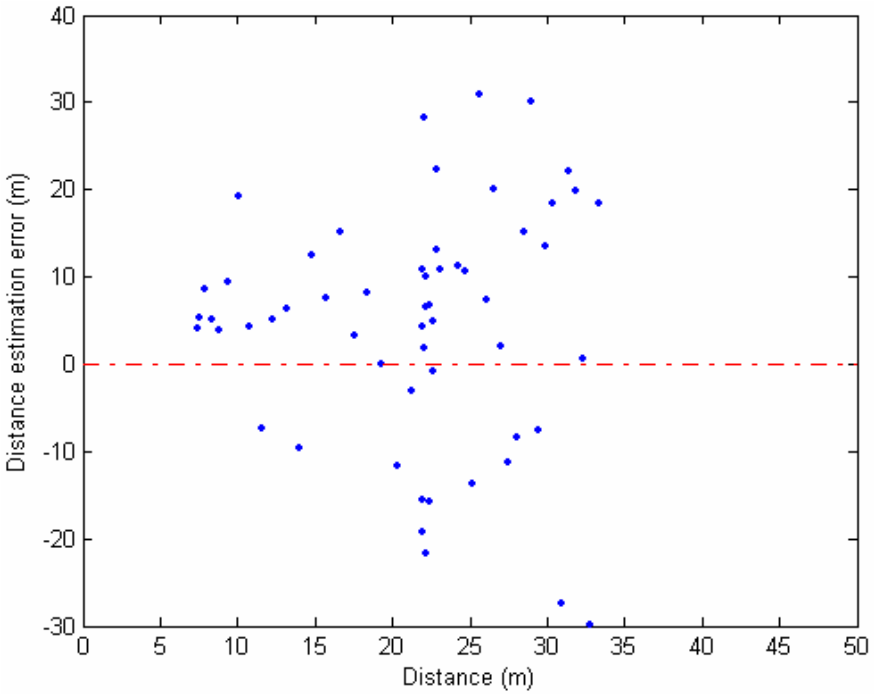

Figure 3.8: Scatter plot of the distance error for Setup 2 at 20 MHz bandwidth.

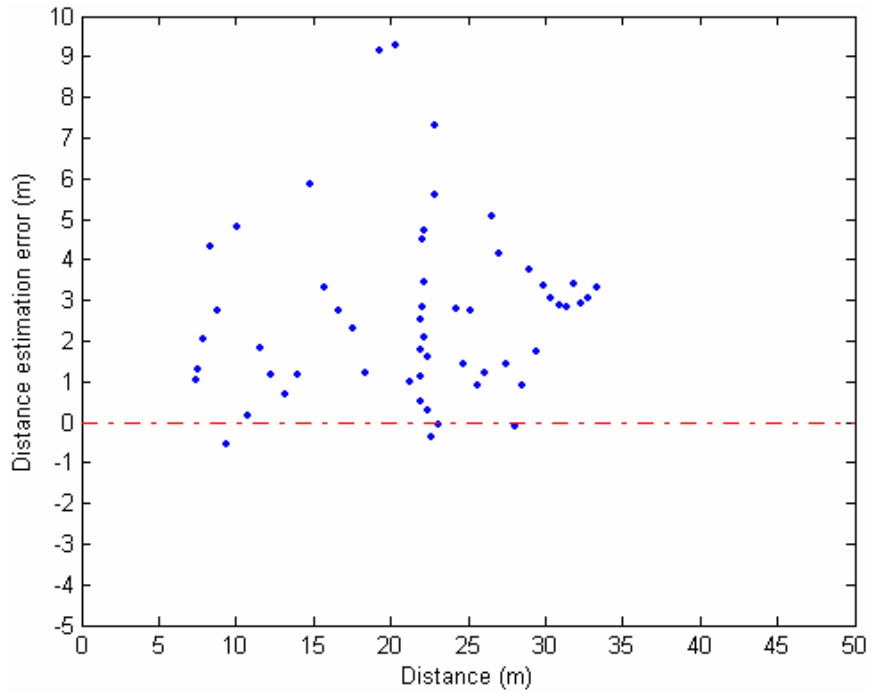

Figure 3.9: Scatter plot of the distance error for Setup 2 at 200 MHz bandwidth.

The distance error decreases at 200 MHz, however there are some error values close to 10 meters in this case which highlights a serious concern for indoor geolocation. One would expect at such a high bandwidth, that the estimation errors might decrease to a reasonable level. However, UDP condition shows that it contributes substantial errors even at higher bandwidths. This phenomenon will be investigated further for the entire measurement database in Chapter 5 along with the effect of different TOA estimation algorithms. Another insightful method to get a better feel for the estimation errors in the different measured areas is the Complementary Cumulative Distribution Function (CCDF). The CCDF for Setup 1 and 2 is computed for different system bandwidths, namely 20, 100 and 200 MHz as illustrated in Fig. 3.10 and 3.11.

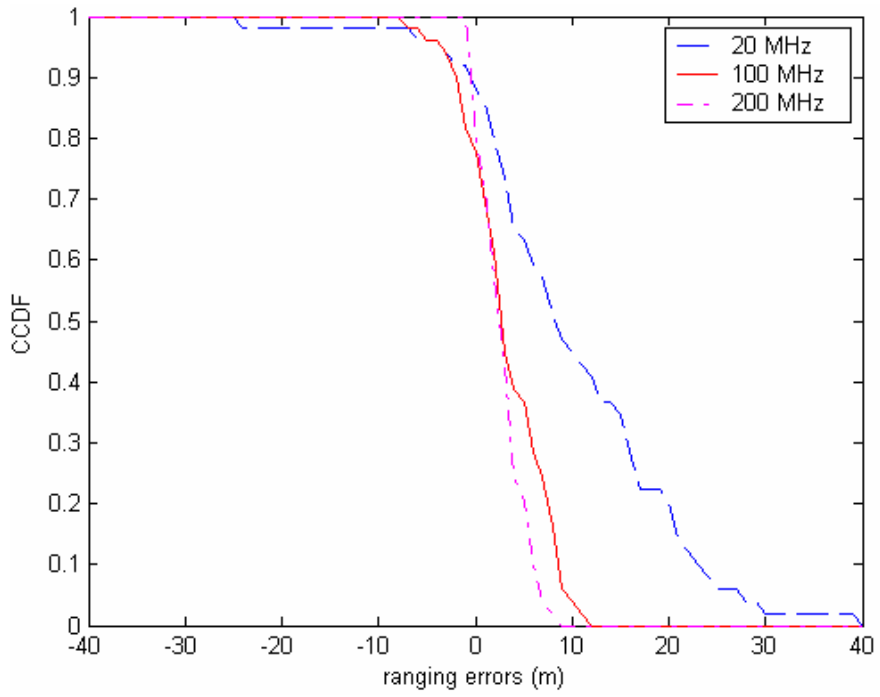

Figure 3.10: CCDF for measurement Setup 1 at 20, 100 and 200 MHz.

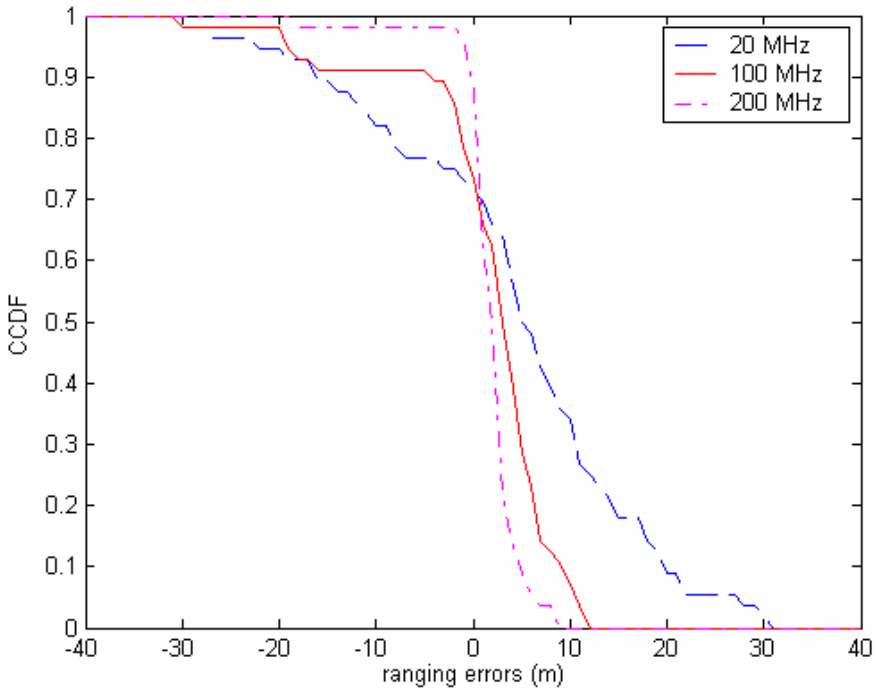

Figure 3.11: CCDF for measurement Setup 2 at 20, 100 and 200 MHz.

3.3 Measurement Database

A measurement database was created by combining previous measurements produced by the CWINS lab and the recent measurement campaign conducted on the third floor of AK building. The previous measurements include the LOS measurements taken on the second and third floor of AK building reported in [9], and mainly OLOS measurements reported in [10].

The LOS measurements were conducted in AK building in rooms 320, 311, 219 and the undergraduate lounge on the first floor. A short description of the measurement site would provide an understanding of the indoor environment. AK 320 is the CWINS

lab and it is much like a typical office environment. It includes office desks, file cabinets and metallic window frames and doors. In addition to the fluorescent lights, many utility pipes and metallic support beams hang from the ceiling. AK 311 is a small conference room that includes blackboards, a desk and several chairs. The space is surrounded by brick walls and metallic window frames and the floor is covered by carpet. AK 219 is located on the second floor of AK and it is surrounded by brick walls and metallic windows. The floor is covered by carpet and the room contains several rows of desks and chairs. The undergraduate lounge is located on the first floor of AK and in addition to the brick walls and the metallic support beams hanging from the ceiling, it contains tables and couches spread across it. The remaining LOS measurements were conducted in Norton Company and they produced 10 points. Norton Company is a manufacturer of welding equipment and abrasives for grinding machines. The building selected for measurement is Plant 7 that is a large building with dimensions in the order of a few hundred meters. This building is connected to a five-floor brick building and to another manufacturing floor through a long corridor. The remainder of Plant 7 is surrounded mainly by open areas and small buildings. Inside the building there are huge ovens, grinding machines, transformers, cranes and other heavy machinery. The building includes a set of partitioned offices with brick external walls, metallic windows and doors attached to the main huge open manufacturing area with steel sheet walls of a height around seven meters and small metallic windows near the ceiling. These sites provided most of the LOS measurement points. This LOS measurement campaign contained a total of 61 points, 54 of which are DDP and only 7 are NDDP. This shows that most of LOS

measurements where no obstructions, such as a wall, are present then the DLOS path is almost always the strongest.

The OLOS measurements were conducted in different sites which included Norton Company, Fuller Laboratory in WPI and WPI Guest House. For all locations, different measurement scenarios were carried out to examine the effects of external and internal walls of the buildings on the channel characteristics. These are indoor to indoor, outdoor to indoor and outdoor to floor. For indoor to indoor both the transmitter and receiver were inside the buildings. For outdoor to indoor the transmitter was placed outside while the receiver was inside the building along different measurement points. For the outdoor to floor, the transmitter was placed outside the building and the receiver was moved into higher floors. Fuller Laboratory is a modern building that houses the Computer Science department at WPI and has been selected as the site for measurements applicable to office areas. The dimensions of this building are on the order of a few tens of meters. The external walls of the laboratory are made of brick with some aluminum siding on the sides, metallic window frames and doors. The internal walls are made of sheetrock and in some offices soft partitions divide the room into cubicles. The WPI Guest house is a big residential house with wooden exterior walls and sheetrock interior walls. The house is very old and some portions of the external walls are made of stone. The house is located in a fairly open area with a few buildings of similar features located nearby. Inside rooms have dimensions in the order of few meters. This OLOS measurement campaign produced 90 points, 10 LOS and 80 OLOS. These 90 points contained 33 DDP, 41 NDDP and only 16 UDP. Thus the lack of UDP justified the need for the UDP measurement campaign. The recent UDP campaign produced 105

measurement points. 49 of those measurement locations are UDP. Another 55 are NDDP and only one measurement point is DDP. Table 3.1 shows the measurement database and the classification breakup.

Table 3.1: Measurement Database

Measurement Campaign	LOS	OLOS	DDP	NDDP	UDP
E. Zand 2003	61	0	54	7	0
J. Beneat et al. 1999	10	80	33	41	16
UDP campaign	0	105	1	55	49
Total (256 points)	71	185	88	103	65

Including the earlier reported CWINS measurements, a total of 256 measurements of which 71 are LOS and 185 are OLOS. Most of LOS cases are DDP and most of OLOS cases are NDDP and UDP. Overall the database contains a total of 65 UDP measurement points along with 103 NDDP and 88 DDP points used for statistical analysis. The measurement database is used in analyzing the performance of different estimation algorithms in those different multipath conditions.

Finally it is important to have a general sense of how DDP, NDDP and UDP compare to each other in terms of distance error. From the 256 measurement points, scatter plots of each condition compare the distance error behavior at 200 MHz. Figure 3.12 shows the scatter plot of DDP distance error at 200 MHz. Most of the measurement errors occur near zero and all of the distance estimation errors are well below 2 meters.

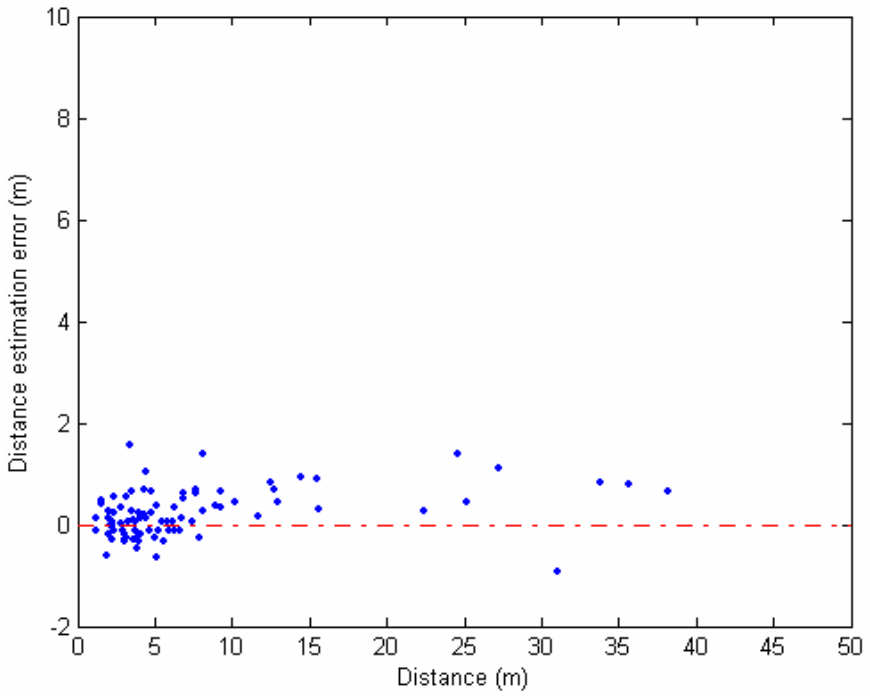

Figure 3.12: Scatter plot of DDP distance error at 200 MHz.

This is very typical of DDP again because of the strong first path and with a high resolution the errors are well contained in this low region. For NDDP, however, error values are much larger than DDP. Figure 3.13 shows the scatter plot of the distance estimation errors.

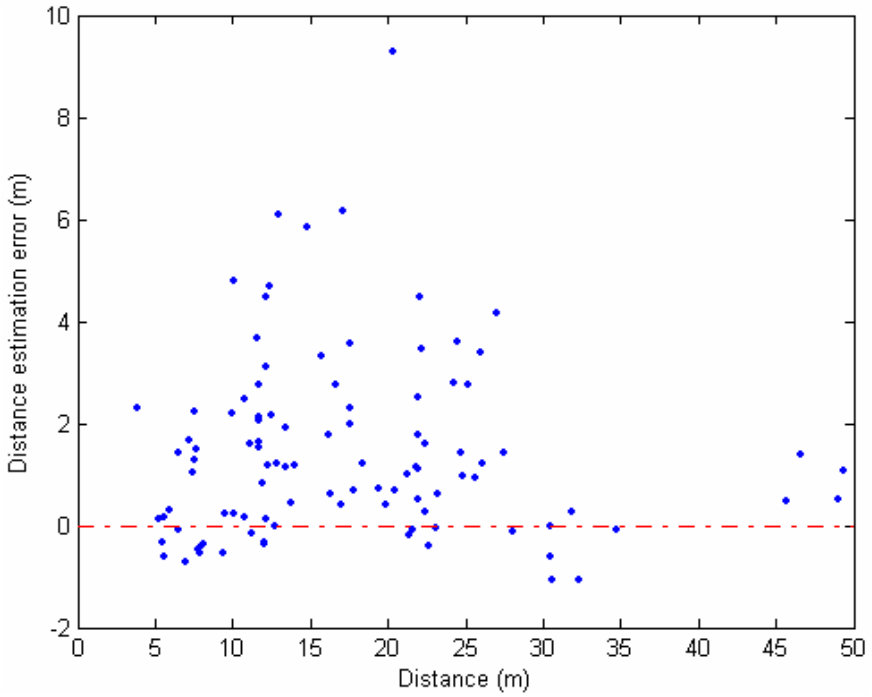

Figure 3.13: Scatter plot of NDDP distance error at 200 MHz.

In this case, NDDP there is a greater fraction of the errors occur between 0 and 4 meters and few errors are more than 6 meters. The presence of the first path here allows its detection but in some instance since the paths arrive in clusters and the peak of the cluster gets detected instead adding to the distance estimation error. In other cases the peak of the cluster is very close to the arrival of the first path and this is illustrated with errors close to zero. Again with 200 MHz bandwidth one would expect that most of the multipath is resolved and that the first path can be detected accurately but this is not the case here. Figure 3.14 shows the distance estimation scatter plot for UDP. Most of the estimation errors here are between 2 and 10 meters as compared with NDDP where most of the errors occurred below 4 meters. From the description of UDP earlier, it seems natural that with the loss of the DLOS path the error values tend to be substantial. Even at

a bandwidth of 200 MHz these errors cannot simply be ignored for indoor geolocation. Notice also that there are few estimation errors close to zero and no errors below zero which shows how the non-existence of a first path causes a shift in the error spread across higher distances. The emphasis of this thesis highlights the UDP problem and evaluates the degree of degradation experienced when falling in such an unfavorable condition. Later in Chapter 5 different estimation algorithms will be applied to the measurement data in order to compare the effect they have on the TOA estimation errors.

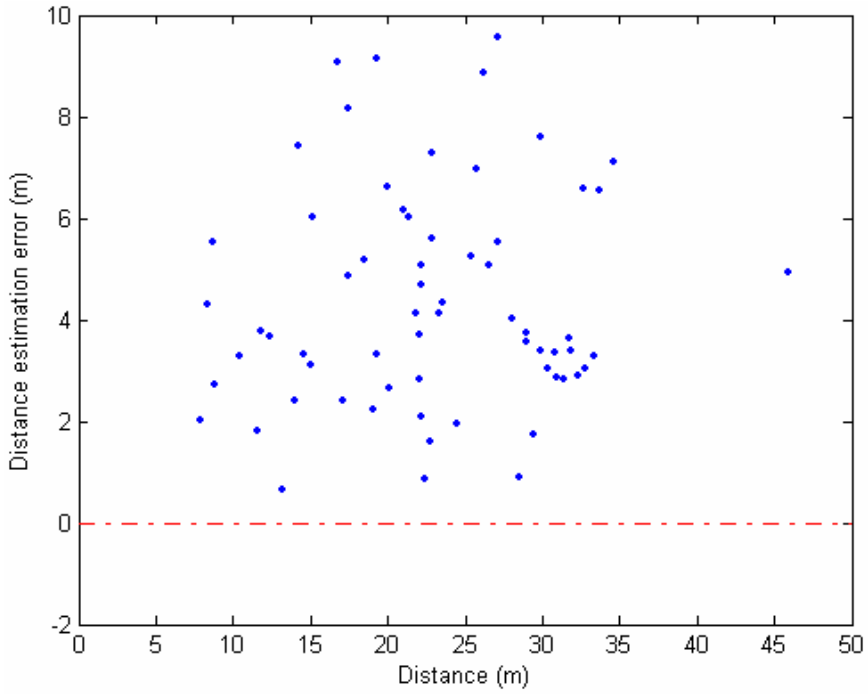

Figure 3.14: Scatter plot of UDP distance error at 200 MHz.

CHAPTER 4 TOA Estimation Algorithms for Indoor Geolocation

The accuracy of TOA estimation is the most important parameter in indoor geolocation. As a result it is essential to examine the factors that affect the accuracy and try to figure out ways to improve it. The harsh indoor multipath is already a limiting factor in deployed geolocation systems. As described in the previous chapter, UDP is a very critical condition that substantially degrades the accuracy of the system. One of the ways to mitigate the problem is to consider behavior of the DLOS path as the bandwidth of the system is changed. It is well known that increasing system bandwidth enhances the time-domain resolution and as a result improve the accuracy of TOA estimation. In situation where the system bandwidth is fixed it is important to find other alternatives to improve the accuracy. One of the practical alternatives is to use post-processing techniques on the frequency domain measurement data. These techniques are the TOA estimation algorithms. In signal processing different algorithms provide different levels of accuracy and in addition, the complexity of implementation is varied as a result. Detecting the DLOS path requires obtaining the time-domain channel profile form the frequency domain measurement data. The following TOA estimation algorithms provide different time domain resolutions that are directly related to accuracy of TOA estimation. These algorithms are used in analyzing the behavior of the first path in different multipath conditions with special attention to UDP.

Section 4.1 introduces the inverse Fourier Transform (IFT) estimation technique and its basic building blocks. Section 4.2 describes the Direct Sequence Spread Spectrum

(DSSS) algorithm. Finally in section 4.3 the theoretical background of the super-resolution algorithm is introduced.

4.1 IFT

A simple and conventional TOA estimation algorithm, IFT provides a time domain representation of the channel profile from the frequency domain measurement data. When the time domain response over part of the time period is desired, the chirp-z transform (CZT) is preferred, providing flexibility in the choice of time domain parameters with the cost of longer computational time as compared with the IFT. Figure 4.1 shows the block diagram of the IFT algorithm.

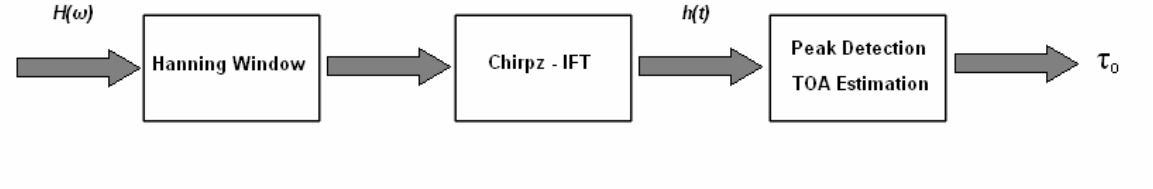

Figure 4.1: Block diagram of IFT estimation algorithm.

As mentioned earlier, prior to application of the CZT, a Hanning window is used to avoid leakage and false peaks by reducing the side-lobes of the time domain response with the cost of reduced resolution. The peak detection algorithm then selects the closest peak to the actual TOA. In this thesis, the term IFT will generally mean application of the CZT unless otherwise stated.

4.2 DSSS

Another estimation algorithm uses the cross-correlation techniques with DSSS signals. In order to simulate DSSS signal-based cross-correlation technique, the frequency response of a raised-cosine pulse with roll-off factor 0.25 is first applied to the frequency domain response as a combined response of band-limitation pulse-shaping filters of the transmitter and receiver. Then, the resultant frequency response is converted to time domain using the IFT for TOA estimation [7]. Figure 4.2 shows the block diagram of the DSSS estimation algorithm. As mentioned earlier, a peak detection algorithm is used to estimate the TOA of the DLOS path.

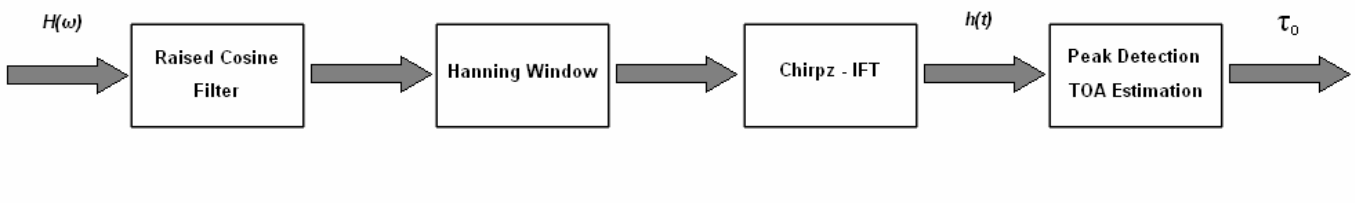

Figure 4.2: Block diagram of DSSS TOA estimation algorithm

4.3 Super-resolution EV/FBCM

The need for higher resolution in the time-domain entails the use of more complicated estimation algorithms. In this thesis, a variant of MUltiple Signal Classification (MUSIC) algorithm is used as a super-resolution technique in TOA estimation for indoor geolocation. The indoor radio channel suffers from severe multipath and the equivalent lowpass impulse response is given by

$$h(t) = \sum_{k=0}^{L_p-1} \alpha_k \delta(t - \tau_k), \qquad (4.1)$$

where L_p is the number of multipath components, $\alpha_k = |\alpha_k| e^{j\theta_k}$ and τ_k are the complex attenuation and propagation delay of the k[th] path, respectively. For example, τ_0 in the above equation is the DLOS path, or the TOA, that needs to be detected for indoor geolocation. The Fourier transform of (4.1) is the frequency domain channel response which is given by

$$H(f) = \sum_{k=0}^{L_p - 1} \alpha_k e^{-j2\pi f \tau_k} \qquad (4.2)$$

The phase of the complex attenuation θ_k is assumed random with a uniform PDF U(0, 2π). Usually these parameters are frequency dependent. However for the frequency bands used in this thesis, the parameters are assumed frequency independent. A harmonic signal model can be created by exchanging the role of time and frequency variables in (4.2) which yields,

$$H(\tau) = \sum_{k=0}^{L_p - 1} \alpha_k e^{-j2\pi f_k \tau} . \qquad (4.3)$$

This model is well known in spectral estimation field [12]. Therefore, any spectral estimation techniques that are suitable for the harmonic model can be applied to the frequency response of multipath indoor radio channel to perform time-domain analysis. In this thesis, a variant of MUSIC algorithm is used as a spectral estimation technique to convert the frequency domain data into the time domain profile needed for determining the DLOS path and TOA.

The discrete measurement data are obtained by sampling the channel frequency response $H(f)$ at L equally spaced frequencies. Considering additive white noise in the measurement, the sampled discrete frequency domain channel response is given by

$$x(l) = H(f_l) + w(l) = \sum_{k=0}^{L_p-1} \alpha_k e^{-j2\pi(f_0+l\Delta f)\tau_k} + w(l), \qquad (4.4)$$

where $l = 0,1,...,L-1$ and $w(l)$ denotes additive white measurement noise with zero mean and variance σ_w^2. The signal model in vector form is

$$\mathbf{x} = \mathbf{H} + \mathbf{w} = \mathbf{V}\mathbf{a} + \mathbf{w} \qquad (4.5)$$

where

$$\mathbf{x} = [\mathrm{x(0)} \quad \mathrm{x(1)} \quad \ldots \quad \mathrm{x(L\text{-}1)}]^{\mathrm{T}}$$

$$\mathbf{H} = [\mathrm{H}(f_0) \quad \mathrm{H}(f_1) \quad \ldots \quad \mathrm{H}(f_{L-1})]\mathrm{T}$$

$$\mathbf{w} = [\mathrm{w(0)} \quad \mathrm{w(1)} \quad \ldots \quad \mathrm{w}(L\text{-}1)]\mathrm{T}$$

$$\mathbf{V} = [\mathrm{v}(\tau_0) \quad \mathrm{v}(\tau_1) \quad \ldots \quad \mathrm{v}(\tau_{\mathrm{Lp-1}})]\mathrm{T}$$

$$\boldsymbol{v}(\boldsymbol{\tau_k}) = [1 \quad e^{-\mathrm{j}2\pi\Delta f\tau k} \quad \ldots \quad e^{-\mathrm{j}2\pi(\mathrm{L}-1)\Delta f\tau k}]\mathrm{T}$$

$$\mathbf{a} = [\alpha_0' \quad \alpha_1' \quad \ldots \quad \alpha_{\mathrm{Lp-1}}']\mathrm{T}$$

$$\alpha_k' = \alpha_k e^{-j2\pi f_0\tau_k}$$

MUSIC super-resolution algorithm is based on eigen-decomposition of the autocorrelation matrix of the signal model in (4.5). The autocorrelation matrix is given by

$$\mathbf{R}_{xx} = E\{\mathbf{x}\mathbf{x}^H\} = \mathbf{V}\mathbf{A}\mathbf{V}^H + \sigma_w^2\mathbf{I} \qquad (4.6)$$

where $\mathbf{A} = E\left\{\mathbf{a}\mathbf{a}^H\right\}$ and superscript H is the Hermitian, conjugate transpose, of a matrix. Since the propagation delays τ_k in (4.1) can be theoretically assumed all different, the matrix V has full column rank which means that the column vectors of V are linearly independent. The $L_p \times L_p$ covariance matrix A is non-singular assuming that $|\alpha_k|$ is constant and the phase is uniform random variable in [0, 2π]. As a result, from the theory of linear algebra, by assuming that $L>L_p$, the rank of the matrix VAV^H is L_p. This means that the $L-L_p$ smallest eigenvalues of R_{xx} are all equal to σ_w^2. The eigenvectors corresponding to $L-L_p$ smallest eigenvalues of R_{xx} are called noise eigenvectors while the eigenvectors corresponding to L_p largest eigenvalues are called signal eigenvectors. Therefore, the L-dimensional subspace that contains the signal vector x is split into two orthogonal subspaces, known as signal subspace and noise subspace, by the signal eigenvectors and noise eigenvectors, respectively [7]. The projection matrix of the noise subspace is then given by

$$\mathbf{P}_w = \mathbf{Q}_w(\mathbf{Q}_w^H\mathbf{Q}_w)^{-1}\mathbf{Q}_w^H = \mathbf{Q}_w\mathbf{Q}_w^H, \qquad (4.7)$$

where $Q_w = [q_{Lp} \quad q_{Lp+1} \quad \dots \quad q_{L-1}]$ and q_k, $L_p \le k \le L-1$, are noise eigenvectors. Since the vector $v(\tau_k)$, $0 \le k \le L_p - 1$, must lie in the signal subspace, we have

$$\mathbf{P}_w\mathbf{v}(\tau_k) = 0. \quad (4.8)$$

Thus the multipath delays τ_k, $0 \le k \le L_p - 1$, can be determined by finding the delay values at which the following MUSIC pseudospectrum achieves maximum value,

$$S_{MUSIC}(\tau) = \frac{1}{\left\|\mathbf{P}_w \mathbf{v}(\tau)\right\|^2} = \frac{1}{\mathbf{v}^H(\tau)\mathbf{P}_w \mathbf{v}(\tau)} = \frac{1}{\left\|\mathbf{Q}_w^2 \mathbf{v}(\tau)\right\|^2} = \frac{1}{\sum_{k=Lp}^{L-1} \left|\mathbf{q}_k^H \mathbf{v}(\tau)\right|^2}. \tag{4.9}$$

In the above analysis, the true or theoretical correlation matrix R_{xx} was considered. In practical implementation, the correlation matrix must be estimated from the measurement data samples. Figure 4.3 illustrates a block diagram of the MUSIC super-resolution TOA estimation algorithm.

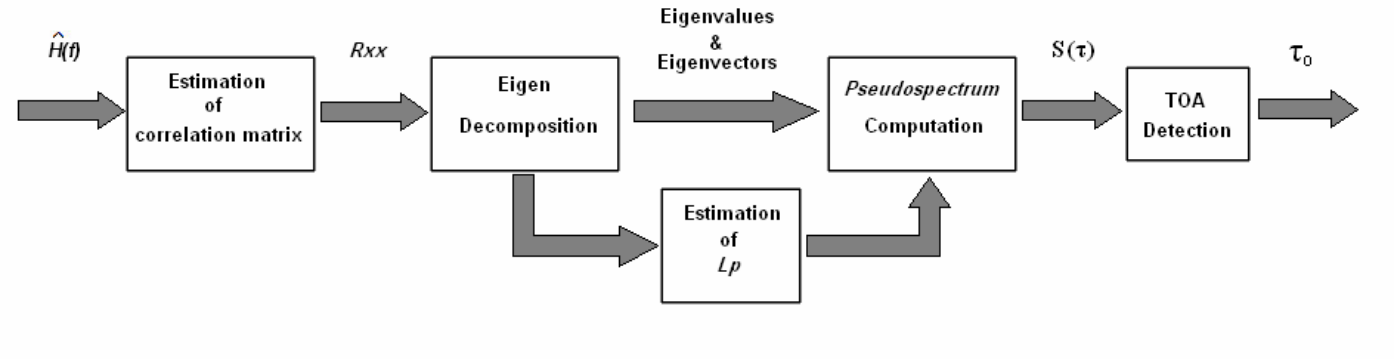

Figure 4.3: Block diagram of MUSIC super-resolution TOA estimation algorithm

The autocorrelation matrix is estimated from the measurement data followed by an eigen-decomposition where the L_p parameters are estimated. Then the pseudospectrum is computed from the Lp parameters, the eigenvectors and the eigenvalues. Once the pseudospectrum is obtained a peak detection algorithm selects the first path and thus the estimate of the TOA. In practical implementations the autocorrelation matrix must be estimated from a limited set of data. As a result with P snapshots of measurement data, estimating the correlation matrix can be obtained from

$$\hat{\mathbf{R}}_{xx} = \frac{1}{P}\sum_{k=1}^{P} \mathbf{x}(k)\mathbf{x}(k)^H. \tag{4.10}$$

However, if only one snapshot of length N is available, then the data sequence is divided into M consecutive segments of length L and then the correlation matrix is estimated as

$$\hat{\mathbf{R}}_{xx} = \frac{1}{M}\sum_{k=0}^{M-1}\mathbf{x}(k)\mathbf{x}(k)^{H}, \qquad (4.11)$$

where M = N – L + 1 and x(k) = [x(k) … x(k + L – 1)]^{T}.

For super-resolution TOA estimation techniques, the measurement data vector x is obtained by sampling the channel frequency response uniformly over a certain frequency band. By selecting the frequency domain sampling interval Δf to satisfy the condition $1/\Delta f \geq 2\tau_{\max}$, where $\tau_{\max}$ is the maximum delay of the measured multipath, it is possible to avoid aliasing in the time domain which is similar to the time domain Nyquist sampling theorem [7].

One assumption that is not valid in actual measurement data is that it is assumed to be stationary. When the data is stationary, the correlation matrix is both Hermitian and Toeplitz (equal elements along all diagonals). However, the estimate of the correlation matrix $\hat{\mathbf{R}}_{xx}$ based on actual measurement data of small finite length N is not Toeplitz. The estimate of the correlation matrix can be improved using the following forward-backward correlation matrix (FBCM),

$$\hat{\mathbf{R}}_{xx}^{(FB)} = \frac{1}{2}(\hat{\mathbf{R}}_{xx} + \mathbf{J}\hat{\mathbf{R}}_{xx}^{*}\mathbf{J}) \qquad (4.12)$$

where the superscript * denotes conjugate, superscript FB stands for forward-backward estimation, and J is the $L \times L$ exchange matrix whose components are zero except for ones on the anti-diagonal. This technique is widely used in spectral estimation with the

name modified covariance method and in linear least-square signal estimation with the name forward-backward linear prediction (FBLP) [12].

Implicitly, in the MUSIC method, the noise eigenvalues are all equal, i.e., $\lambda_k = \sigma_w^2$ for $L_p \le k \le L-1$, which means that the noise is white. In practice, when the correlation matrix is estimated from the limited measurement data samples, then the noise eigenvalues are not equal. To deal with this issue a slight variation on the MUSIC algorithm is introduced which is known as the eigenvector (EV) method [7]. The pseudospectrum is defined as

$$S_{EV}(\tau) = \frac{1}{\sum_{k=L_p}^{L-1} \frac{1}{\lambda_k} \left| \mathbf{q}_w^H \mathbf{v}(\tau) \right|^2}, \qquad (4.13)$$

where $\lambda_k, L_p \le k \le L-1,$ are the noise eigenvalues. Effectively the pseudospectrum of each eigenvector is normalized by its corresponding eigenvalue. The EV method is identical to the original MUSIC if all the noise eigenvalues are equal. The performance of the EV method is less sensitive to inaccurate estimate of the parameter L_p, which is highly desirable in practical implementation [12]. In this thesis, the EV method with FBCM was used to estimate the TOA of the DLOS path. EV/FBCM refers to the type of MUSIC algorithm applied throughout the thesis unless otherwise stated.

CHAPTER 5 Performance Analysis in Different Indoor Multipath Conditions

In TOA based indoor geolocation systems, the most important parameter is the accuracy of distance estimation. There are several factors that affect the accuracy of estimation which include the multipath condition, the TOA estimation algorithm used and the bandwidth of the system. In the multipath condition, the behavior of the DLOS path is important. It ranges from a strong path to an undetected first path; therefore, the accuracies vary accordingly. In addition the power of the strongest path and the power of the paths close to the DLOS path also affect the accuracy. It was clearly shown in Chapter 3 that one of the difficult challenges that face geolocation system designers is the phenomenon of UDP. In these areas the error is significant and it is important to know how much error it actually introduces. The other multipath conditions such as DDP and NDDP also warrant considerable attention especially at lower bandwidths. It is necessary to analyze how the TOA accuracy varies for those different conditions. The bandwidth of the system is also an important factor in the accuracy of TOA. In general, as the bandwidth increases the distance measurement error decreases. However, for the so called UDP conditions the system exhibits substantially high distance measurement errors that can not be eliminated with the increase in the bandwidth of the system. At the same time it is interesting to see how much resolution and TOA estimation improvement an increase in bandwidth provides for the different multipath conditions. Once a certain limitation has been established with the bandwidth of the system and the inherint

multipath condition, TOA estimation algorithms can further improve the accuracy. Chapter 4 introduced different TOA estimation algorithms. They range from the basic IFT to the more complex super-resolution. The use of these algorithms in enhancing the time-domain resolution is different. The cost of improved resolution in time-domain is a longer computational time. The performance analysis of these algorithms and the behavior of the DLOS path in different multipath conditions provide an insight into the different factors affecting the TOA estimation. The algorithms' capabilities and limitations in improving the accuracy help in establishing quantitative boundaries on the accuracy of estimation errors.

In this chapter, the TOA estimation algorithms along with the comprehensive measurement database are used for statistical analysis. The main focus here is the accuracy of distance estimation which is directly related to TOA of the DLOS path. In Section 5.1, the performance of distance error in LOS with OLOS is compared. Then the geolocation specific multipath conditions such as DDP, NDDP and UDP are also compared in the same section. Section 5.2 examines the performance of the estimation algorithms in these different multipath conditions. Specifically, traditional estimation algorithms such as IFT and DSSS are compared with super-resolution algorithm (EV/FBCM) in different indoor environments. In addition, the effect of system bandwidth on the TOA estimation errors is described in Section 5.3.

5.1 TOA Estimation Errors in Different Multipath Conditions

As mentioned earlier the behavior of TOA estimation varies significantly in different multipath conditions. Two categories will be discussed in this section where the

method of classification is different. The behavior of TOA estimation in a physical obstruction based classification, namely LOS and OLOS will be analyzed. After that, a geolocation based classification which focuses on the DLOS path behavior will be analyzed. All the analysis is based on the measurement database mentioned in Chapter 3. For the LOS and OLOS, the database is divided according to the existence of a physical obstruction between the transmitter and receiver. For the geolocation classification, the database is divided according to the strength of the DLOS path, regardless of the obstruction. In other words, a measurement profile where an obstruction exists in the DLOS path might be classified as DDP if the first path is the strongest.

5.1.1 LOS vs OLOS

Comparing the two different environments, the performance of an indoor geolocation system varies substantially. The absence of any significant obstructions in the DLOS path provides LOS scenarios with an advantage in terms of mean of ranging error. The significant difference between them is apparent. The obstruction of the first path in OLOS causes substantial error when compared to LOS case. Figure 5.1 shows the mean and standard deviation (STD) of ranging error in different system bandwidths for both LOS and OLOS cases.

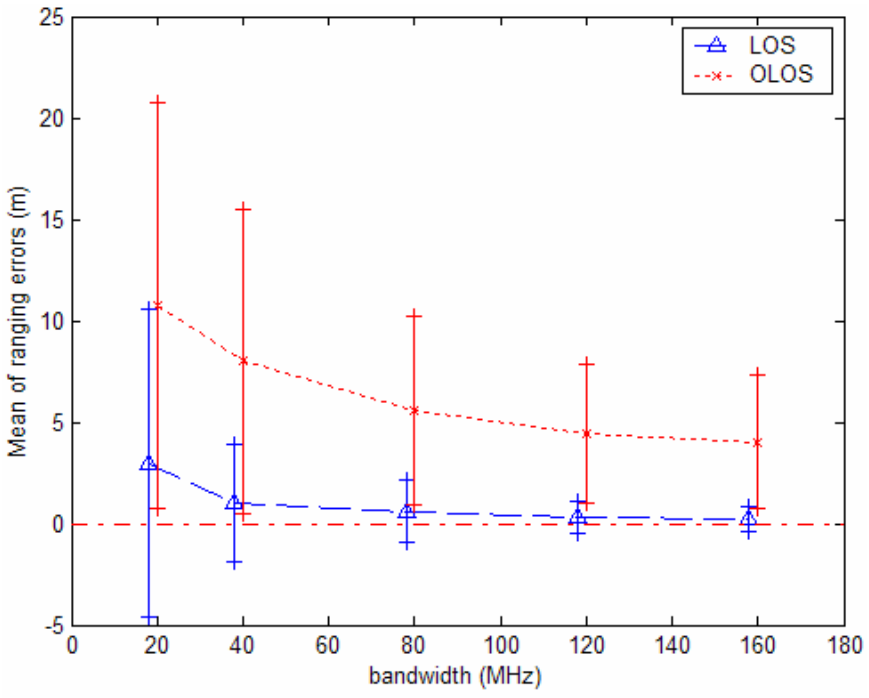

Figure 5.1: Mean and STD of ranging errors for LOS and OLOS environments. The vertical lines denote the STD around each mean value.

Notice the substantial error inherent in OLOS case as opposed to LOS. One observation here is that the ranging error decreases with increasing system bandwidth. Again higher system bandwidth provides higher time-domain resolution and thus better TOA estimation. Notice how the LOS ranging errors approach zero with increasing system bandwidth. On the other hand for OLOS this is simply not the case. This occurs because as the bandwidth increases, the multipath effect is removed and the ability to resolve the different paths improves. However for OLOS cases, even with an improved ability to resolve the multipath the strength of the DLOS path introduces major limitations in accuracy of estimation. For instance, at 20 MHz OLOS suffers a mean error of 10.7 m while LOS has an error of 2.9 m. As the bandwidth increases, LOS error

approaches zero and in the case of 160 MHz it is 0.2 m while OLOS still exhibits a significant 4.1 m error.

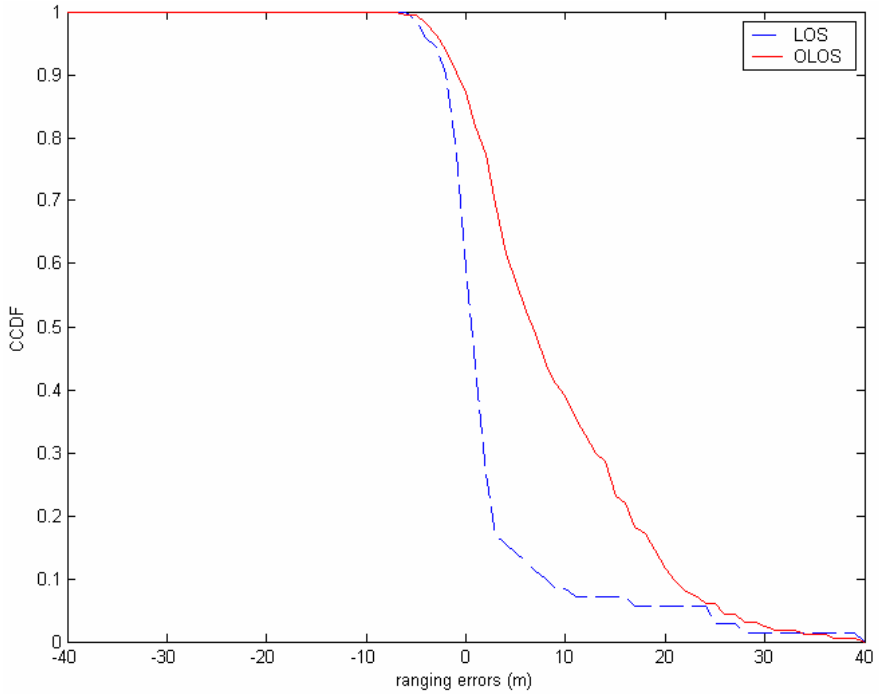

Figure 5.2: Complementary CDF of ranging errors in LOS and OLOS environment at 20 MHz bandwidth.

A more insightful way to compare the behavior of TOA estimation errors in those conditions is to examine the CCDF. Figure 5.2 shows the CCDF of ranging errors for LOS and OLOS at 20 MHz bandwidth. Notice how OLOS exhibits substantial ranging errors compared to LOS. The power of the DLOS path is the distinguishing factor in the performance. Figure 5.3 shows the CCDF of ranging errors for both cases at 160 MHz. In this case the TOA estimation is further improved.

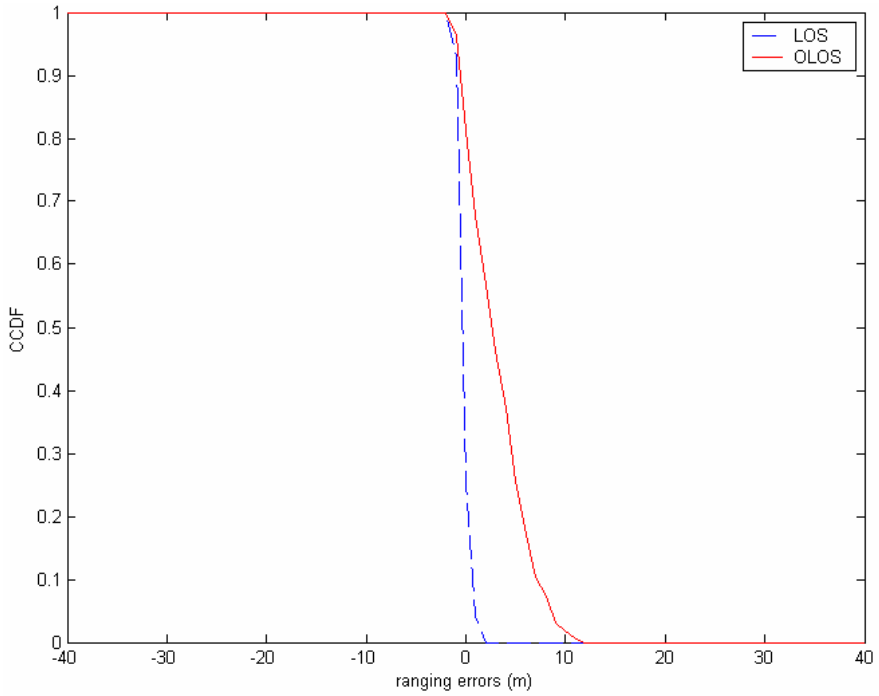

Figure 5.3: Complementary CDF of ranging errors in LOS and OLOS environment at 160 MHz bandwidth.

The ranging error is reduced significantly for the LOS case. Similarly, for the OLOS the accuracy of estimation improves even further, but still there is a significant gap between the two scenarios. In general, OLOS is a combination of NDDP and UDP where the DLOS path is not the strongest and in some cases it is not detected. This introduces substantial error values that cannot be mitigated by increasing the system bandwidth. In fact later in the chapter the performance of TOA estimation will be analyzed for the unfavorable UDP case and it will be shown how the bandwidth ceases to have an effect on the estimation error after a certain value.

5.1.2 DDP, NDDP & UDP

In the previous section it was evident that OLOS introduces substantial TOA estimation errors. Although this might provide an indication about the behavior of the TOA estimation errors, the analysis does not provide sufficient insight into the statistics of the DLOS path. A geolocation based classification is therefore more accurate in depicting what happens to the ranging errors according to the condition inherent on the first path. In this type of categorization there are three cases, namely DDP, NDDP and UDP. The measurement database was divided according to the strength and availability of the DLOS path. With the loss of DLOS path, UDP causes major problems for accurate TOA estimation. As a result, the mean and STD of the distance error are expected to be significant when compared to other cases such as DDP or NDDP. Figure 5.4 shows the mean and STD of the ranging error for UDP compared to DDP and NDDP using IFT algorithm. It is clear that the mean of ranging error for UDP is substantially larger than the two other cases. In fact at 20 MHz, UDP has a mean error that is 5 times that of DDP and 1.5 times that of NDDP.

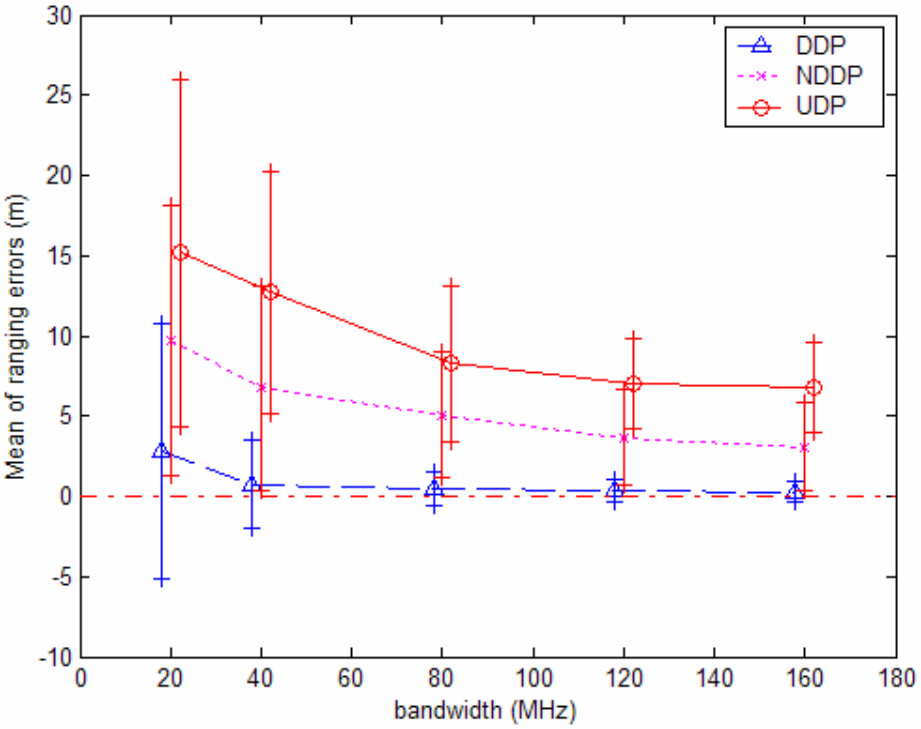

Figure 5.4: Mean and STD of ranging errors for DDP, NDDP and UDP multipath conditions. The vertical lines denote the STD around each mean value.

As the bandwidth increases UDP continues to exhibit significant error values. For example at 160 MHz the mean of distance error for UDP is almost 7 meters while DDP is a mere 0.29 meters. The STD for DDP drops drastically with increasing bandwidth when compared to the other two conditions. Similarly, with increasing bandwidths the STD also decreases for NDDP and UDP. Figure 5.5 shows the CCDF of ranging errors for the different multipath conditions which provide additional insightful comparison.

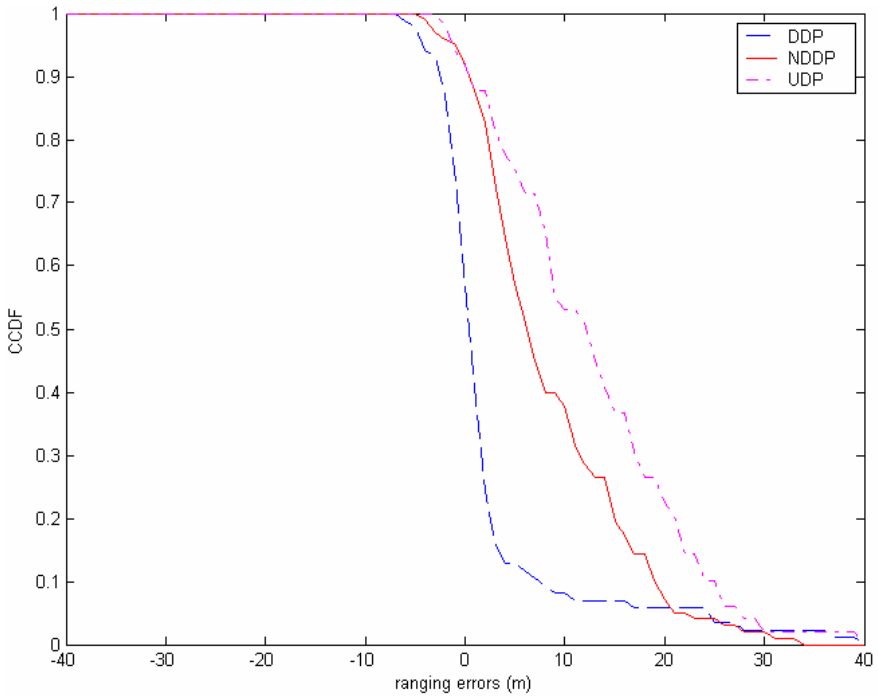

Figure 5.5: CCDF of ranging errors for DDP, NDDP and UDP multipath conditions at 20 MHz bandwidth.

In order to understand the reason for the different ranging errors introduced by the multipath conditions it is important to think in terms of the multipath and the strength of the DLOS path. For example for DDP, the first path is always the strongest and the multipath is almost completely resolved at higher bandwidths. For NDDP, however the case is different. The first path is never the strongest and the multipath introduces the majority of error in the estimation. The paths arrive in clusters and the higher bandwidth splits those clusters into corresponding paths, but still the weakness of the DLOS path causes additional errors. For UDP the main issue here is the unavailability of the first path. It is rather intuitive that without the first path the error is the greatest among the other multipath conditions. Nevertheless, with increases in system bandwidth the

multipath is further resolved, however the first path is still unavailable and as a result this introduces the most substantial ranging error. Figure 5.6 shows the CCDF of ranging errors at a higher bandwidth.

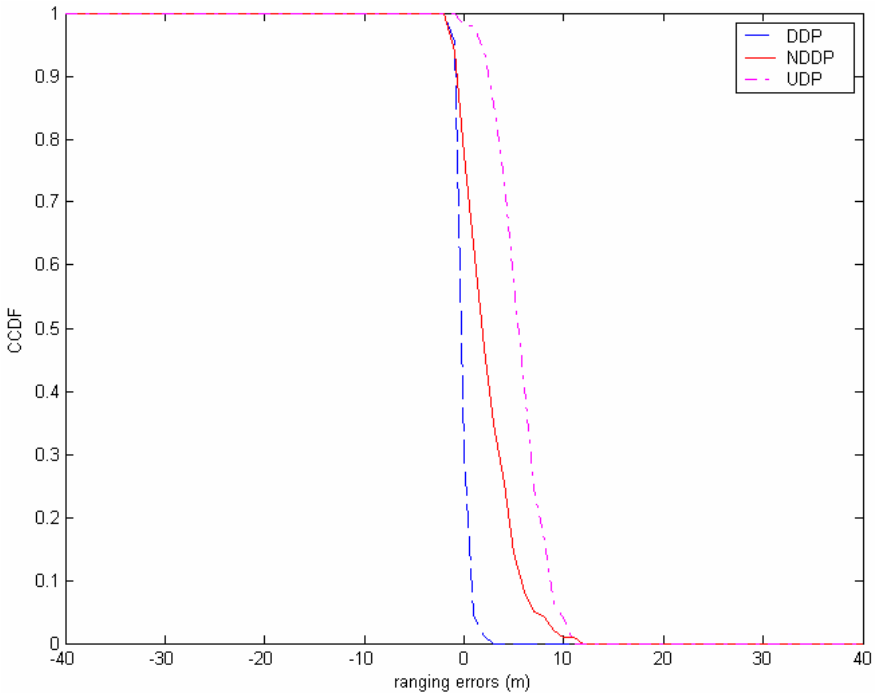

Figure 5.6: CCDF of ranging errors for DDP, NDDP and UDP multipath conditions at 160 MHz bandwidth.

Comparing the two CCDF at different bandwidths shows the improvement in ranging accuracy from 20 to 160 MHz. However still at the higher bandwidth UDP exhibits the highest ranging errors among the multipath conditions. It is important to note that the accuracy of TOA estimation is substantially degraded when a receiver moves from a DDP position to an NDDP or UDP. As will be discussed later, better TOA

estimation algorithms reduce average distance error but have limitations for UDP. The loss of the DLOS path creates a situation where a large distance error is unavoidable even with an increase in the bandwidth of the system.

5.2 Analysis of different TOA estimation algorithms

In practical implementation both the system bandwidth and the multipath condition at a certain instant will be fixed. Accordingly a certain estimation error will impose limitations on the capability of the geolocation system. The question here is whether with a given set of constraints such as the bandwidth of the system and the multipath environment it would be possible to further reduce the error and enhance the accuracy of estimation. Introducing more complex TOA estimation algorithms might alleviate the substantial ranging errors inherent in the harsh indoor environment. However other concerns arise. How will the estimation algorithms behave in the different multipath conditions? Exactly how much improvement in accuracy of estimation will they provide? Do they provide same improvements in lower system bandwidth as opposed to higher system bandwidths? All these questions are valid when comparing different estimation algorithms for indoor geolocation.

In this section the performance of the TOA estimation algorithms, namely IFT, DSSS and EV/FBCM which were described in Chapter 4 will be analyzed for different bandwidths, multipath conditions and scenarios. First following the structure of the pervious section, a comparison is carried out between LOS and OLOS conditions. Then the algorithms are put to the test in the geolocation specific multipath conditions. The statistical analysis should provide a quantitative insight into the capabilities of the

algorithms to improve TOA estimation errors in regards to the multipath condition and the bandwidth of the system.

5.2.1 LOS vs. OLOS

The performance of the three TOA estimation algorithms IFT, DSSS and EV/FBCM, is compared for two different scenarios and several bandwidths. In LOS environment, the performance of the algorithms in terms of mean of ranging error is very close to each other. Figure 5.7 illustrates mean and standard deviation values in LOS for the three algorithms in different bandwidths.

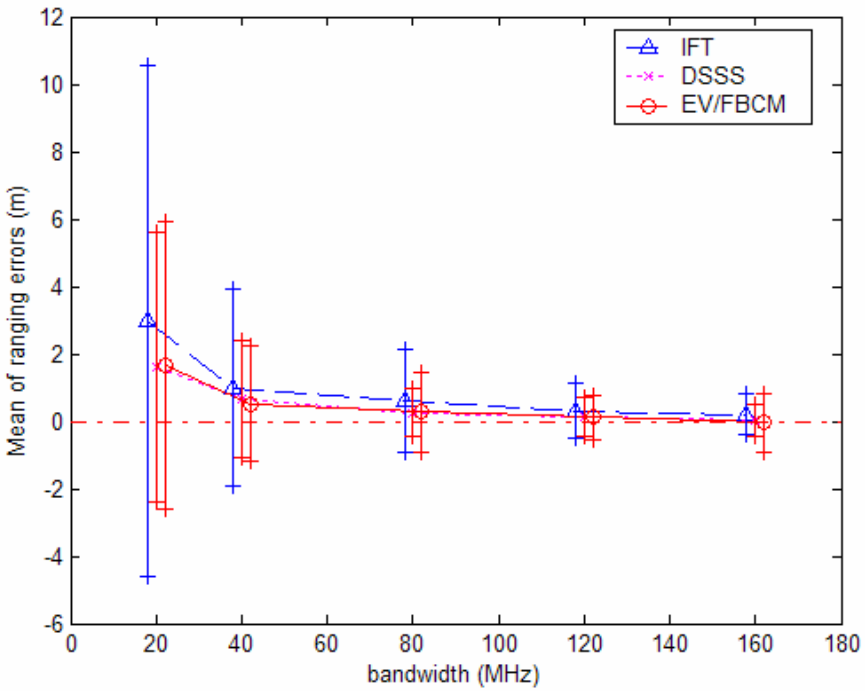

Figure 5.7: Mean and STD of ranging errors in LOS using different TOA estimation algorithms.

At lower bandwidths, EV/FBCM performs slightly better than IFT but almost the same as DSSS. At higher bandwidths, the distance error approaches zero and there is no significant advantage for either algorithms. The STD also decreases significantly with increasing bandwidth. As a result, it is apparent that in LOS conditions with strong DLOS path and higher system bandwidths the use of more complex estimation algorithms does not provide an advantage.

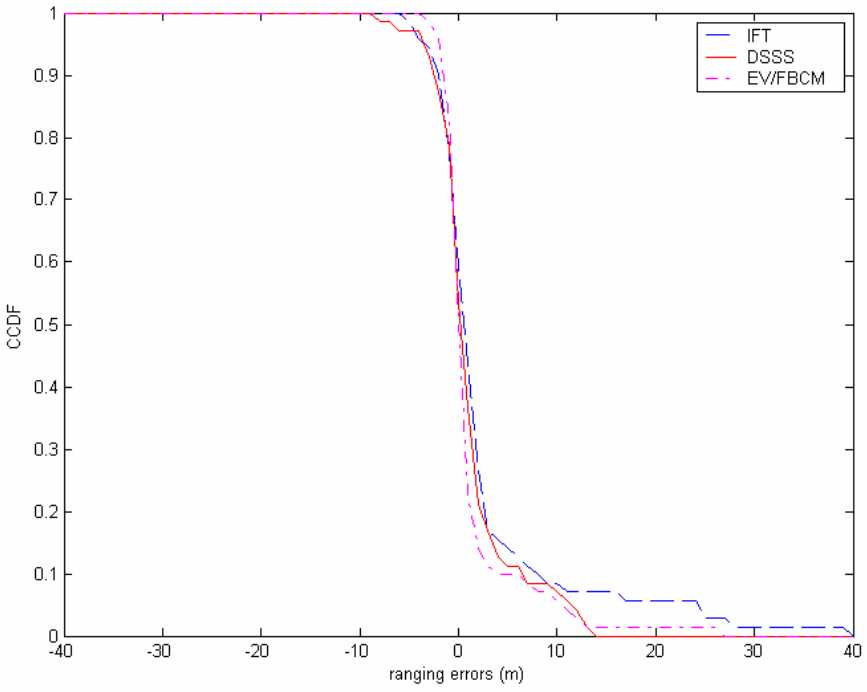

Figure 5.8: CCDF of ranging errors for LOS using different TOA estimation algorithms at 20 MHz bandwidth.

At 20 MHz bandwidth, Fig. 5.8 shows compares the CCDF of the three TOA estimation algorithms in LOS scenario where it shows how EV/FBCM provides slight advantage compared to the other two algorithms. The super-resolution technique provides a better time-domain resolution and thus detects the DLOS path more accurately especially at lower bandwidths. Although the LOS scenario exhibits relatively low error values, the EV/FBCM has the ability to further reduce the error to accurately detect the first path. Figure 5.9 shows the CCDF of ranging errors at 160 MHz bandwidth. In general as was observed in the previous section, at higher bandwidths, LOS ranging errors tend to approach zero.

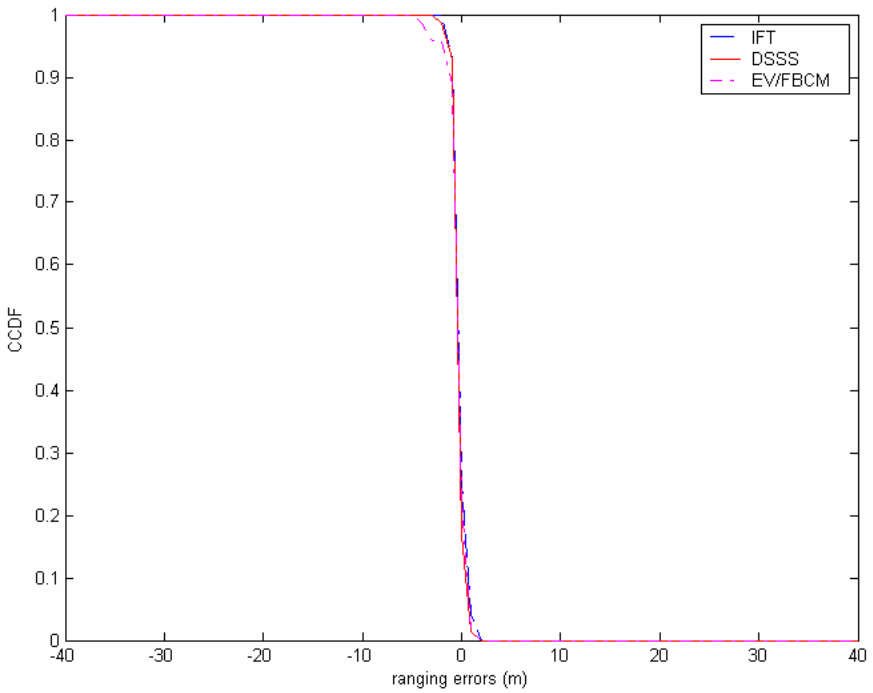

Figure 5.9: CCDF of ranging errors for LOS using different TOA estimation algorithms at 160 MHz bandwidth.

As a result the significance of the TOA estimation algorithms is even further diminished. In other words, for this scenario and at high system bandwidths, the performance of the estimation algorithms is close to each other and they do not provide significant enhancement in the time-domain resolution because it is rather sufficient. A couple of observations are warrant for discussion. First the algorithms closely fit each other in terms of TOA estimation. Second, in practical implementation for LOS situations with a large system bandwidth it is sufficient to accurately detect the first path. Introducing complex estimation algorithms only introduce longer computational time and are not necessary, in fact they can become counterproductive.

In OLOS scenario, the first path suffers attenuation from walls and other obstructions. As a result the DLOS path is rarely the strongest and that introduces problems for detection. In addition the multipath condition is more severe adding further inaccuracies into the behavior of the ranging error. This is shown in Fig. 5.10 where the distance error for all the algorithms is worst than the LOS case. The EV/FBCM algorithm significantly improves the TOA estimation and, in addition, it outperforms the other conventional algorithms as evident from the figure.

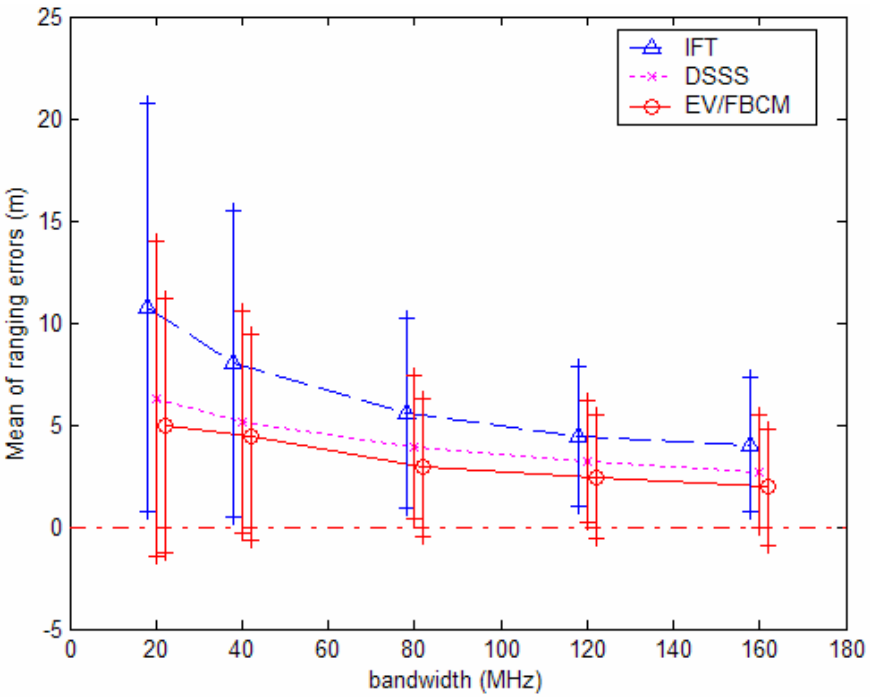

Figure 5.10: Mean and STD of ranging errors in OLOS using different TOA estimation algorithms. The vertical lines correspond to plus and minus one STD about the mean.

As a result, in obstructed conditions more complex TOA estimation algorithms provide means to reducing the error and are necessary for indoor geolocation. At 20 MHz the mean of ranging error for IFT is 10.71 m while it is 6.28 m and 4.96 m for DSSS and EV/FBCM respectively. At 160 MHz the ranging error drops significantly and EV/FBCM has the superior performance with error value around 1.9 m while IFT and DSSS are trailing with 4.0 m and 2.71 m respectively.

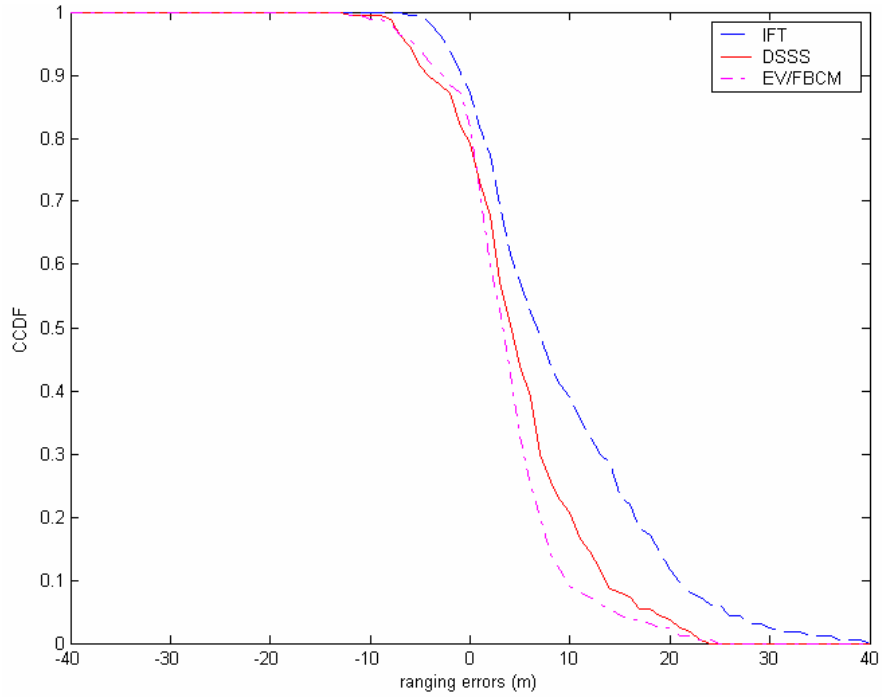

Figure 5.11: CCDF of ranging errors for OLOS using different TOA estimation algorithms at 20 MHz bandwidth.

For OLOS, EV/FBCM exhibits the best performance and it is indeed necessary in TOA estimation since it provides twofold decrease in the error when compared to the traditional IFT algorithm. Figure 5.11 shows the CCDF of the three algorithms for OLOS at 20 MHz bandwidth. IFT exhibits the worst performance. DSSS provides better estimation accuracy since it has a higher time-domain resolution. However at this bandwidth, EV/FBCM outperforms the other algorithms. Figure 5.12 shows the CCDF of the three algorithms at a higher bandwidth.

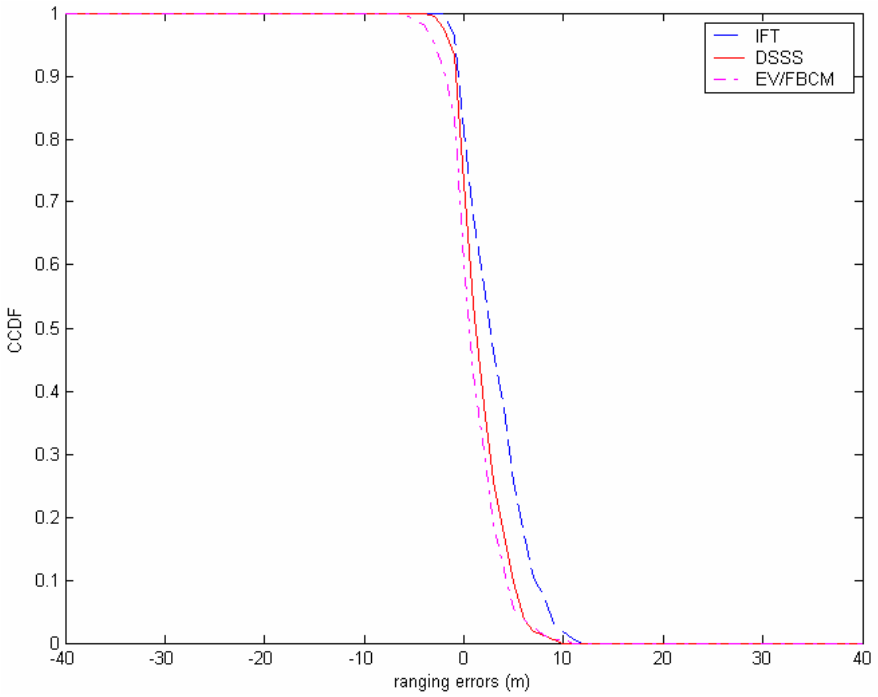

Figure 5.12: CCDF of ranging errors for OLOS using different TOA estimation algorithms at 160 MHz bandwidth.

As the overall estimation error decreases, EV/FBCM provides better accuracy even at higher bandwidths. As a result, super-resolution algorithms are necessary in OLOS environments since they provide substantial improvement of estimation accuracy. On the other hand, use of those algorithms does not provide significant improvement to the TOA estimation in LOS environment, especially at high system bandwidths.

5.2.2 DDP, NDDP & UDP

With the second main classification, similarly, the effectiveness of the algorithms is different in each condition. Figure 5.13 shows the mean and STD performance of the

algorithms in DDP. This is very similar to the LOS case because most of the LOS are DDP, but some of the OLOS are DDP.

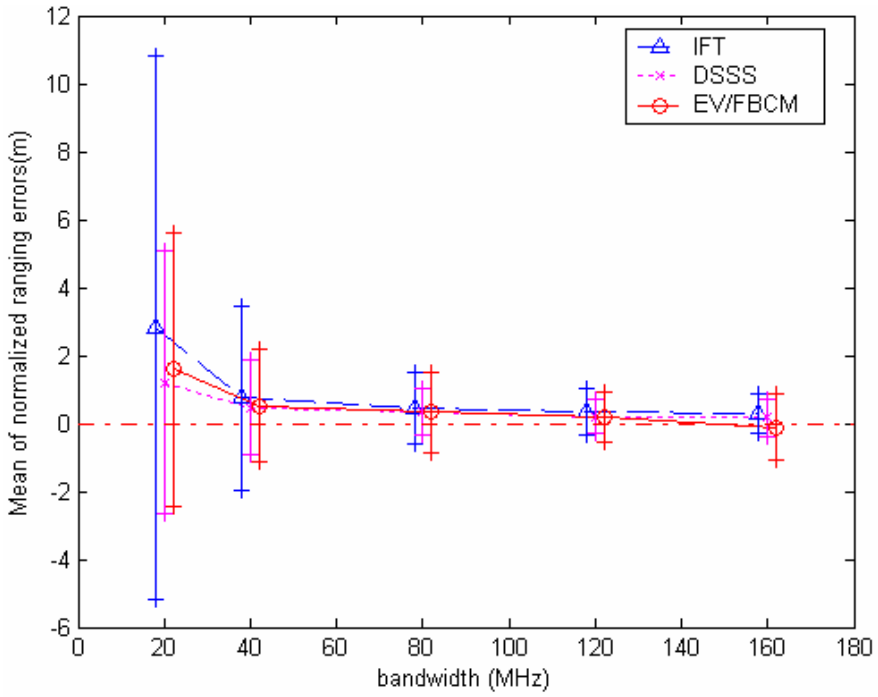

Figure 5.13: Mean and STD of ranging errors in DDP using different TOA estimation algorithms. The vertical lines correspond to plus and minus one STD about the mean.

In order to better understand the behavior of the algorithms in DDP it is helpful to examine a measured channel profile. Figure 5.14 shows a DDP channel profile at 40 MHz illustrating the performance of the three algorithms. The vertical dash-dot line is the expected TOA. Notice that the DLOS is detected successfully for the three algorithms. EV/FBCM views the time domain channel profile with a higher resolution and thus it

provides better accuracy in detection. However the improvement provided is vital at lower bandwidths but negligible at higher bandwidths.

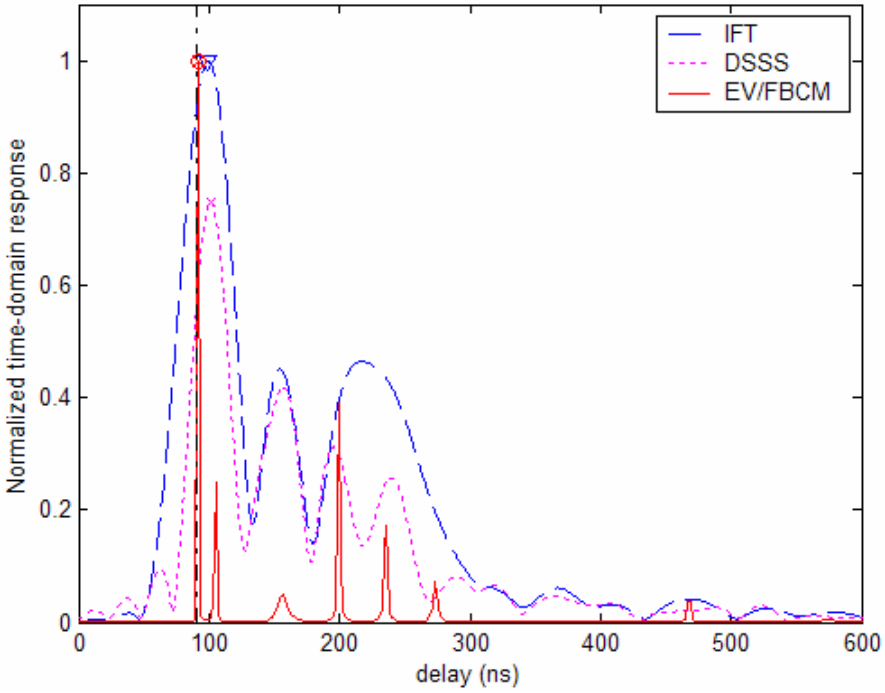

Figure 5.14: Measured DDP profile obtained with three estimation algorithms at 40 MHz bandwidth.

Similarly the CCDF provides another insight into the performance of the algorithms in this specific multipath condition. Two examples will be illustrated next. The first one is Fig. 5.15 which provides the CCDF of ranging error at 20 MHz while Fig. 5.16 shows the CCDF at 160 MHz of bandwidth. This condition is very close to LOS in that at lower bandwidths the super-resolution algorithm provides slight advantage, while at higher bandwidths it fails to provide any concrete improvement.

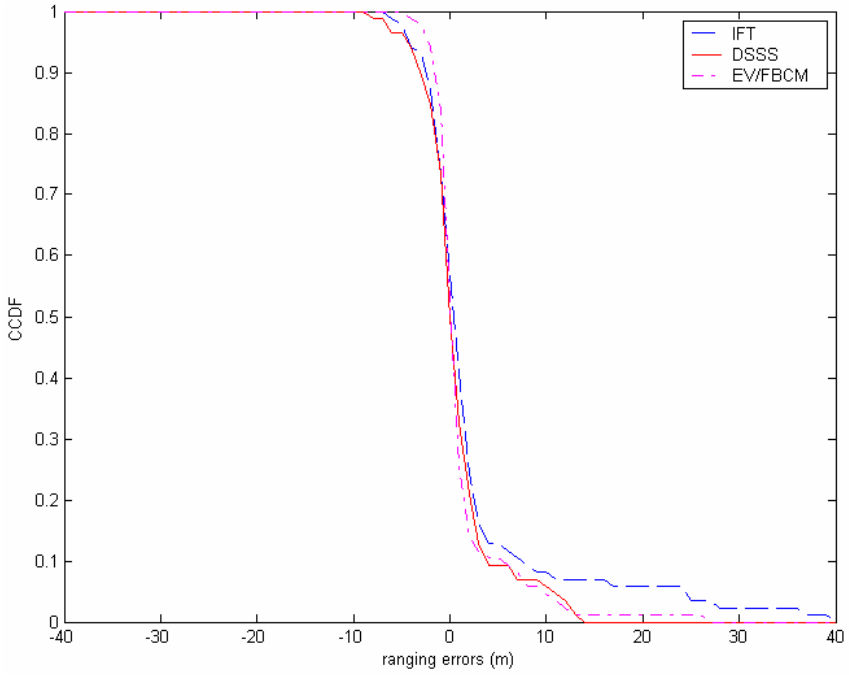

Figure 5.15: CCDF of ranging errors for DDP using different TOA estimation algorithms at 20 MHz bandwidth.

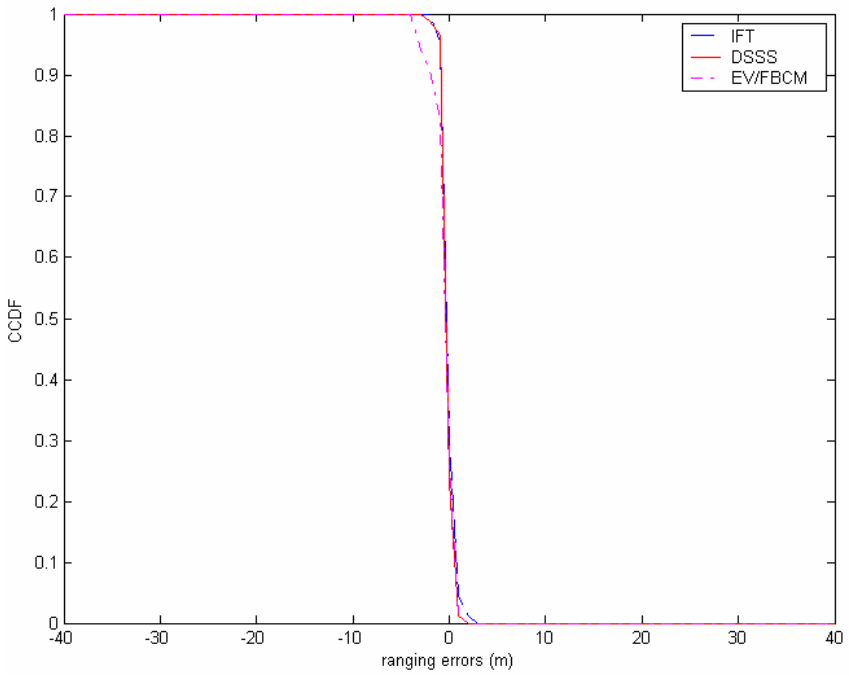

Figure 5.16: CCDF of ranging errors for DDP using different TOA estimation algorithms at 160 MHz bandwidth.

In NDDP, Fig. 5.17 shows that EV/FBCM algorithm performs significantly better than the other two algorithms. The main reason is that it has the ability to view the channel profile with higher resolution. In this category the first path usually combines with the subsequent paths and forms a cluster. The conventional algorithms detect the peak of the cluster as the DLOS path and hence the TOA. This erroneous detection causes serious problems for TOA estimation. The higher resolution of the EV/FBCM algorithm "splits" the cluster and provides other paths not detected conventionally. In some cases, the algorithm detects the DLOS path; in other the second or even the third is detected. Regardless of the path detected, Fig. 5.17 shows that on average EV/FBCM exhibits lower mean of ranging error when compared to the other algorithms.

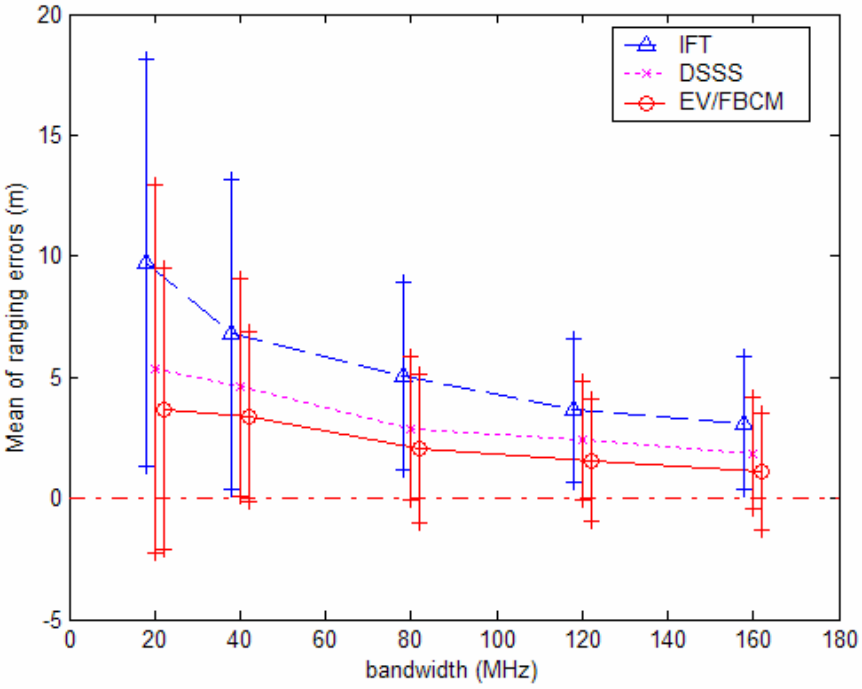

Figure 5.17: Mean and STD of ranging errors in NDDP using different TOA estimation algorithms. The vertical lines correspond to plus and minus one STD about the mean.

The performance of EV/FBCM in this condition can be justified by examining Fig. 5.18, which shows a typical NDDP profile. The vertical dash-dot line is the expected TOA and it is clear how both the IFT and the DSSS are unable to detect the correct path. However EV/FBCM resolves the cluster and reduces the TOA error by detecting a closer path and in this case it actually detects the first path. Overall it is true to say that in NDDP conditions EV/FBCM provides the best performance in terms of mean of ranging errors.

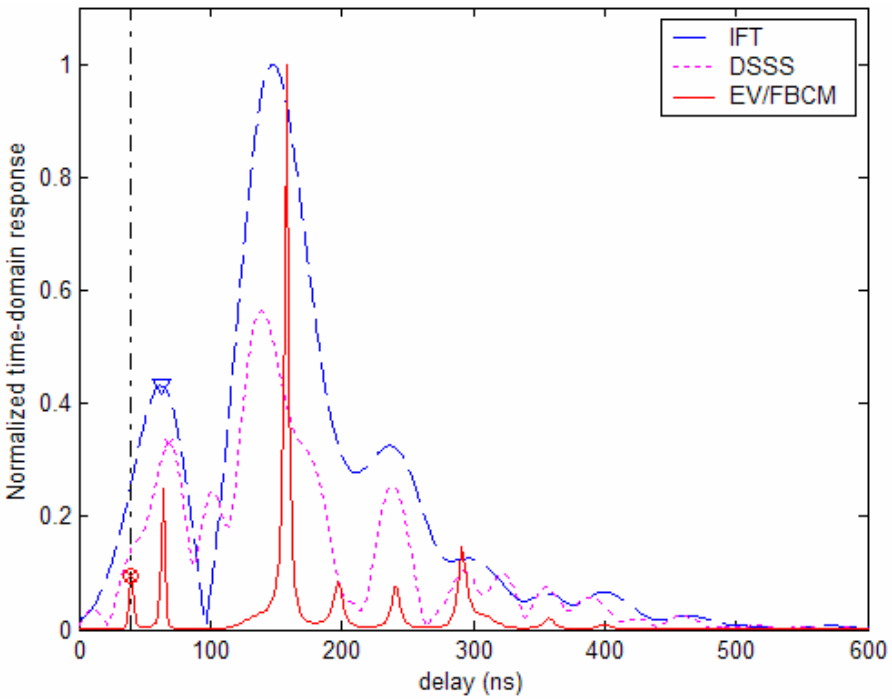

Figure 5.18: Measured DDP profile obtained with three estimation algorithms at 40 MHz bandwidth.

In addition, the CCDF of the estimation algorithms for NDDP condition shows how the EV/FBCM indeed has the ability to resolve multipath and reduce the estimation error. The super-resolution algorithm has the ability to combat multipath effect; however the strength of the first path becomes an additional factor into the error values. In some cases, the first path is detectable but very weak which causes additional errors that cannot be remedied by the algorithms or the bandwidth of the system. Figure 5.19 shows the CCDF for the algorithms in NDDP at 20 MHz.

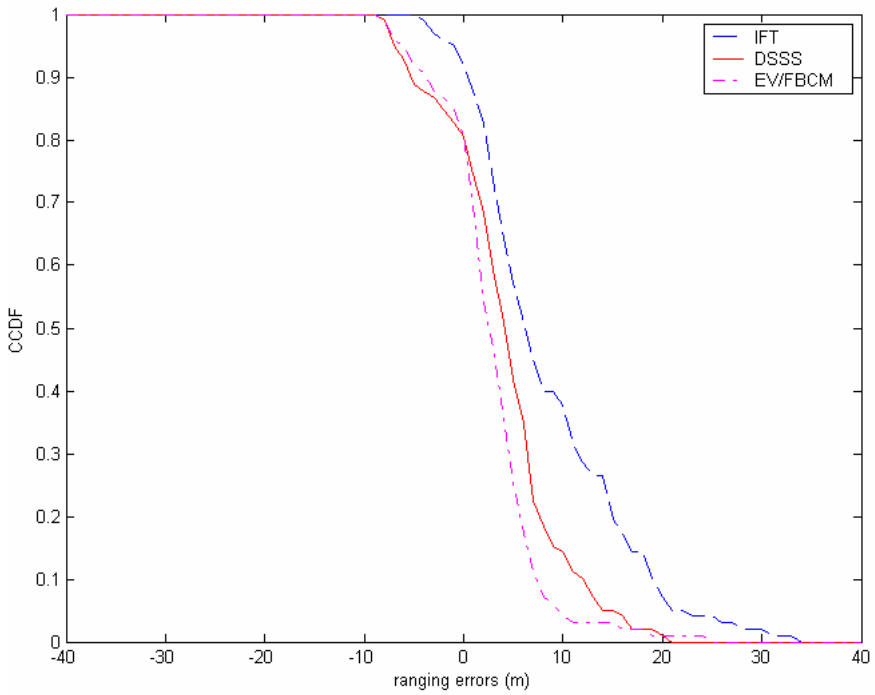

Figure 5.19: CCDF of ranging errors for NDDP using different TOA estimation algorithms at 20 MHz bandwidth.

In most cases however, for NDDP the performance enhancement provided by EV/FBCM is necessary for indoor geolocation applications. Figure 5.20 provides CCDF at 160 MHz. Notice how EV/FBCM improves detection while IFT trails with the worst performance. DSSS has a higher resolution than IFT but cannot compare with EV/FBCM. The trade-off here is a higher computational time for EV/FBCM compared to the other algorithms. It is possible to conclude that EV/FBCM has the best performance in NDDP conditions even at higher system bandwidths.

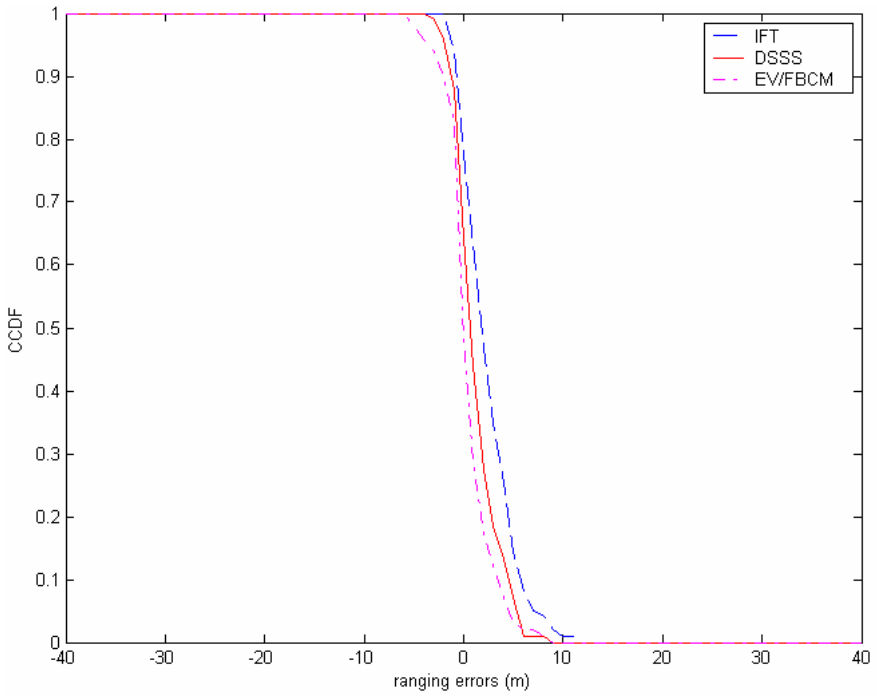

Figure 5.20: CCDF of ranging errors for NDDP using different TOA estimation algorithms at 160 MHz bandwidth.

In UDP scenarios, EV/FBCM provides an advantage compared to the other algorithms. Although the DLOS path does not exist, nevertheless, EV/FBCM is expected to perform better than the other algorithms. Figure 5.21 shows the mean and STD of ranging error for UDP conditions. On average, the EV/FBCM outperforms the other algorithms and exhibits lower error even at higher bandwidths.

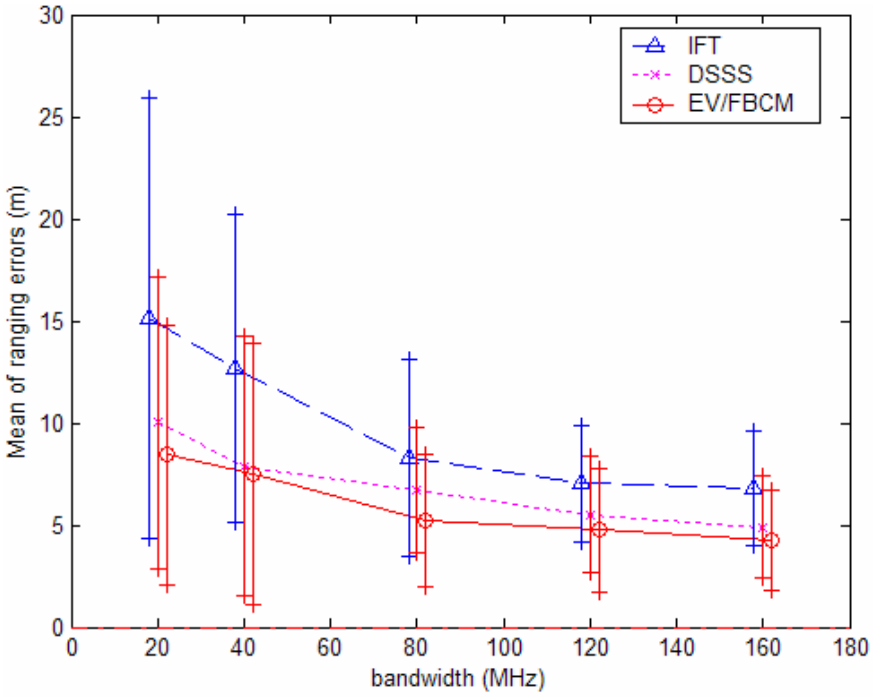

Figure 5.21: Mean and STD of ranging errors in UDP using different TOA estimation algorithms. The vertical lines correspond to plus and minus one STD about the mean.

By examining a UDP measurement sample, it is possible to see how the three algorithms compare. Figure 5.22 shows a measured UDP profile with the absence of the first path. It is clear that EV/FBCM detects a closer path and improves the TOA estimation when compared to IFT and DSSS.

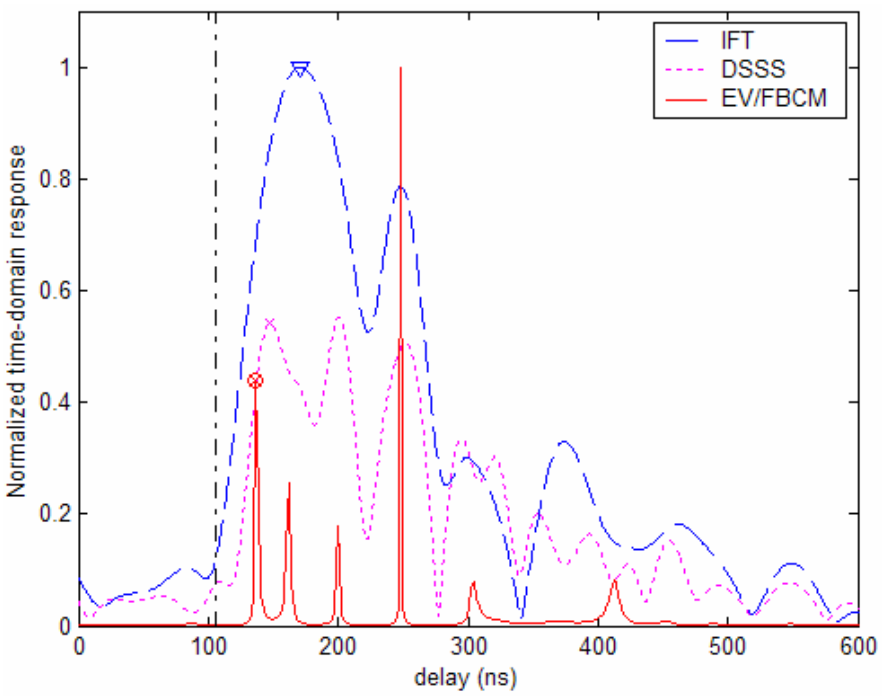

Figure 5.22: Measured UDP profile obtained with three estimation algorithms at 40 MHz bandwidth.

The weakness of the DLOS path makes it difficult to resolve the multipath and detect it. As a result, the UDP condition introduces unavoidable errors and regardless of the bandwidth or the estimation algorithm used, the positioning system will exhibit substantially large errors. This degraded performance requires that in the deployment of an indoor geolocation system care must be taken to avoid coverage areas with UDP conditions. This will further reduce the error and enhance the accuracy of TOA detection and estimation. This is further justified by the CCDF curves in Fig. 5.23 and Fig. 5.24 which show the behavior of the algorithms at two different system bandwidths.

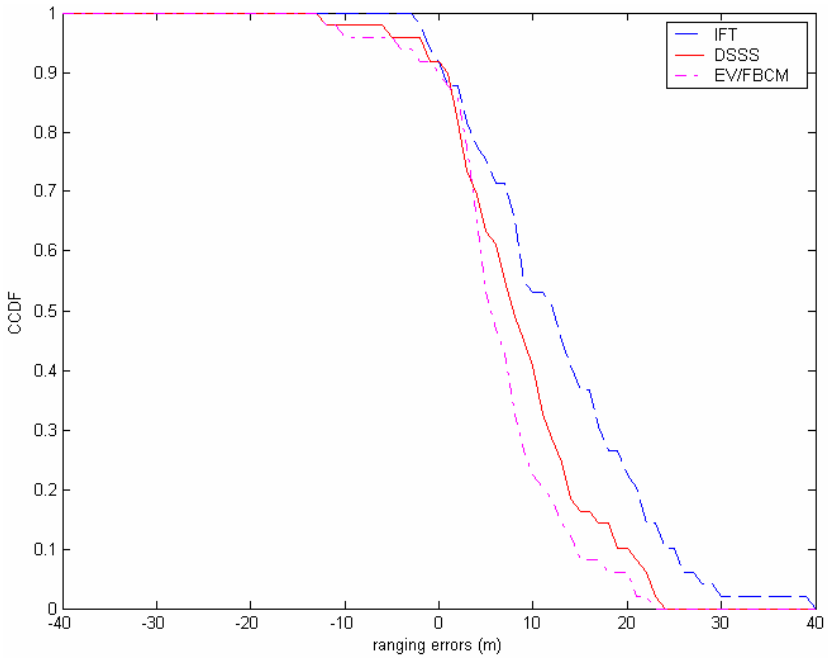

Figure 5.23: CCDF of ranging errors for UDP using different TOA estimation algorithms at 20 MHz bandwidth.

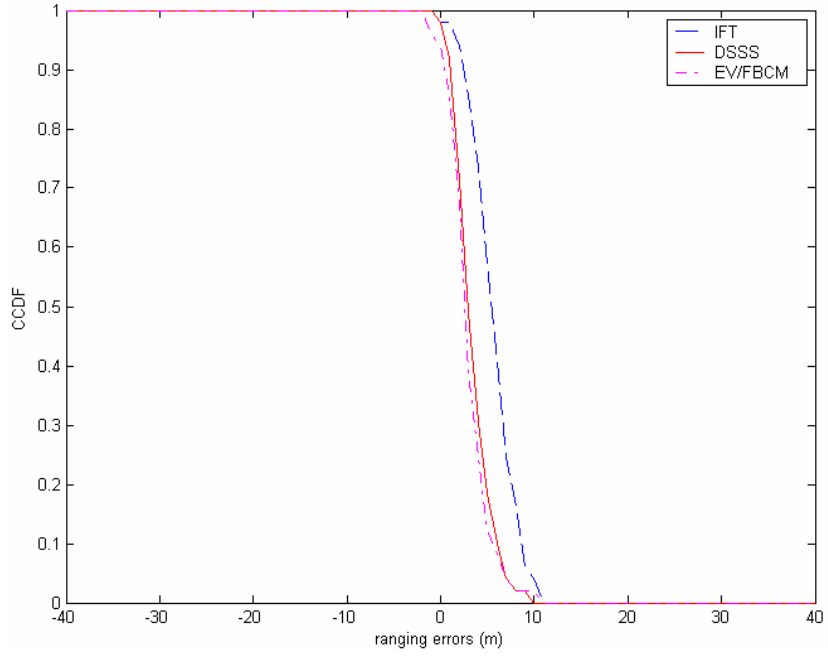

Figure 5.24: CCDF of ranging errors for UDP using different TOA estimation algorithms at 160 MHz bandwidth.

5.3 System Bandwidth

Finally after assessing the performance of the different estimation algorithms and their effect on the multipath conditions, it is important to analyze the effect of system bandwidth on UDP. A general fact that has been noticed in the analysis section is that when the bandwidth of the system increases, the estimation error reduces due to enhanced time-domain resolution. It is thus important to see if in fact increasing system bandwidth would help in mitigating the UDP problem. For the other conditions, system bandwidth significantly enhances the estimation of the DLOS path. Figure 5.25 shows a plot of absolute distance error for the three multipath conditions with varying system bandwidths.

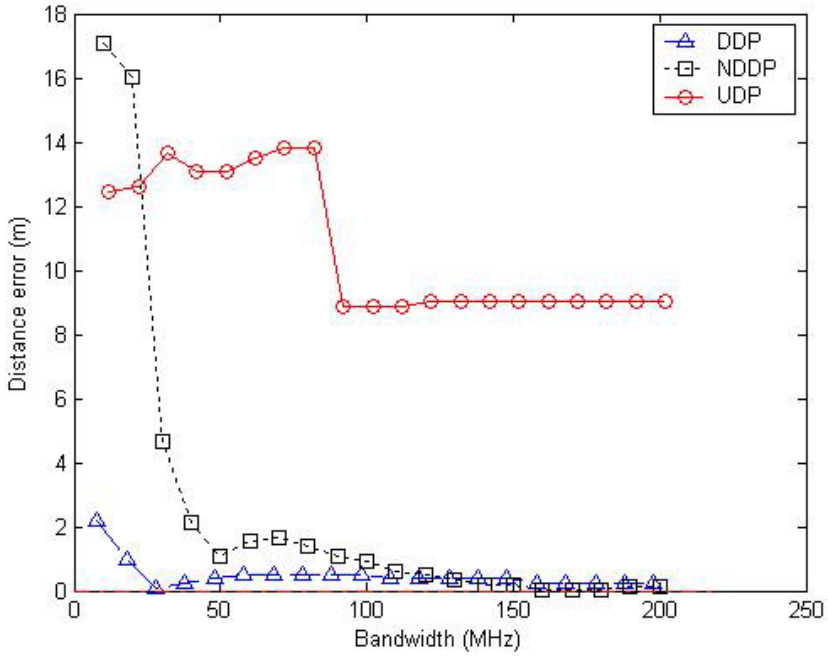

Figure 5.25: Effect of system bandwidth on absolute distance error for the three multipath profiles DDP, NDDP and UDP.

Notice how the DDP drops to exhibits error values below 2 m and then drops significantly after 30 MHz. For NDDP the error drops from 18 meters to around 1.5 meters at 50 MHz. By the time it reaches 200 MHz the error rolls off to zero. At higher bandwidths the effect of the multipath is reduced significantly and that is the reason why both DDP and NDDP eventually exhibit error values close to zero. Since they have a detected first path the distance estimation is not hindered by other problems at higher bandwidths. Unfortunately such encouraging results cannot be concluded about UDP. The increases in bandwidths have limited effects. In fact after 100 MHz, the error stays around the same value of 8.5 meters which is a very significant cost in indoor geolocation. As a result it is possible to see that this adverse condition introduce serious problems in detecting the first path. In this case, after certain increases in the bandwidth of the system, the multipath effect is reduced significantly but the unavailability of DLOS path still causes a problem. In other words, the distance error stops responding to further increases in bandwidth. Finally it is evident that the use of super-resolution algorithms provides slight enhancement in the error levels. Likewise, the bandwidth of the system has limitations in improving the TOA estimation error especially for the UDP case.

CHAPTER 6 Conclusions and Future Work

6.1 Conclusions

In this thesis, the performance of TOA estimation algorithms in different multipath conditions was analyzed based on the measurement database described in Chapter 3. The measurement database includes measurements conducted with a focus on the important UDP condition. After analyzing the data and examining the different statistical results it is noteworthy to mention the following conclusions.

First, the measurement campaign targeted on the UDP condition produced significant UDP measurements which are very useful for statistical analysis and performance comparison with different multipath conditions. It was illustrated that the estimation error in such unfavorable condition is significant and provides a serious challenge to indoor geolocation system designers. In addition the geolocation-specific classification of DDP, NDDP and UDP provides a better insight into analyzing the behavior of the first path which is more important in geolocation application. Second, UDP conditions introduce unavoidable TOA estimation errors even with increasing the bandwidth of the system and applying super-resolution algorithm. When comparing the different indoor multipath conditions, DDP provides the best error performance because of the strength of the DLOS path. For NDDP, however, performance varies substantially between low and high bandwidths where the latter provide means of reducing the effect of multipath. In all indoor measurement conditions, increasing the bandwidth of the system provides an increase in the estimation accuracy and thus enhancement in distance estimation. This has a limitation for UDP since it stops responding to bandwidth changes

after a certain limit. Finally, the super-resolution EV/FBCM algorithm provides no significant advantage in DDP. It has the best performance in NDDP conditions and it enhances distance estimation in UDP. It is also more significant for lower system bandwidths since it provides a much needed higher-time domain resolution.

6.2 Future Work

Since this research area is fairly new, there are many different and important ways to contribute to indoor geolocation science and technology. There is a need for comprehensive measurements and modeling for indoor geolocation specific applications. As such the emerging UWB technology promises a solution for combating the indoor multipath condition. As a result the implementation of UWB measurement system and indoor channel modeling for positioning is an important area for further research. In addition, analyzing the effect of bandwidth on the distance error could be accomplished by examining bandwidths in excess of 6 GHz. The following can also be conducted as a continuation of the research work, namely, comparing the performance of super-resolution algorithms to the UWB system for indoor geolocation.

Appendix A Additional CCDF plots in different bandwidths

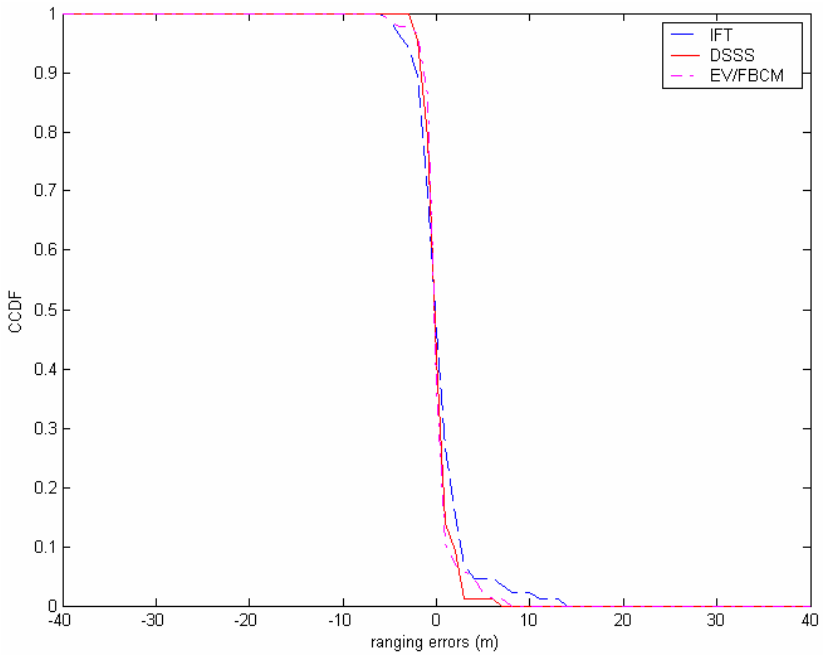

Figure A.1: CCDF Algorithm performance analysis for DDP at 40 MHz bandwidth.

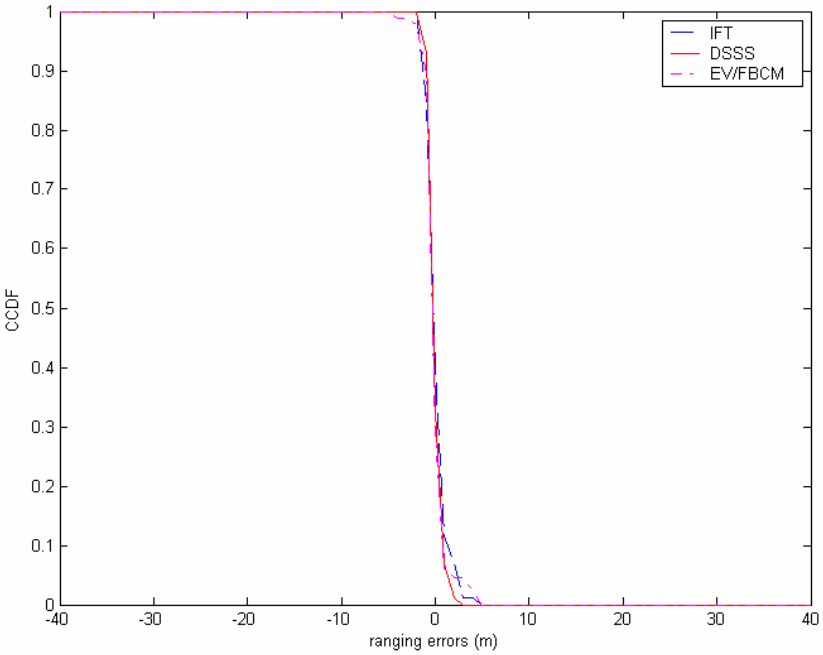

Figure A.2: CCDF Algorithm performance analysis for DDP at 80 MHz bandwidth.

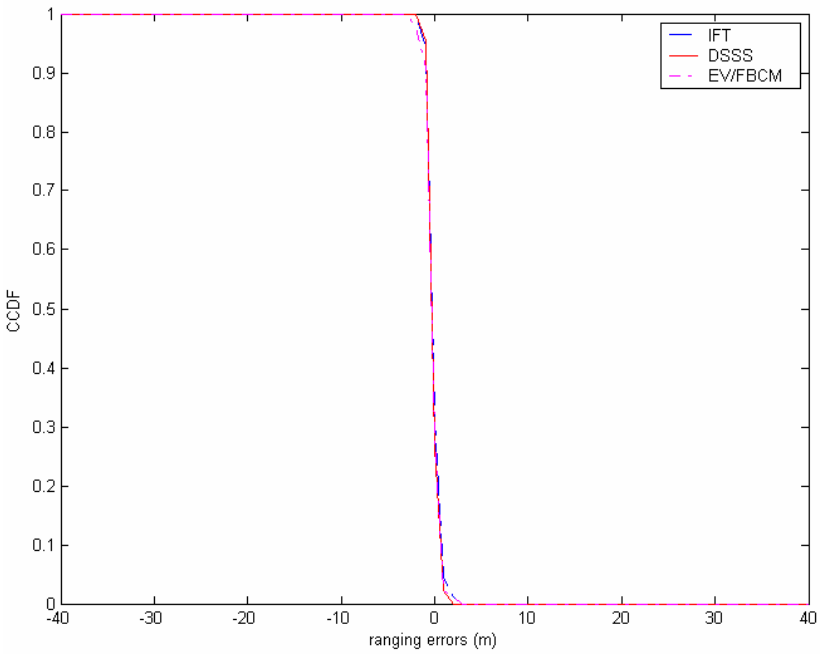

Figure A.3: CCDF Algorithm performance analysis for DDP at 120 MHz bandwidth.

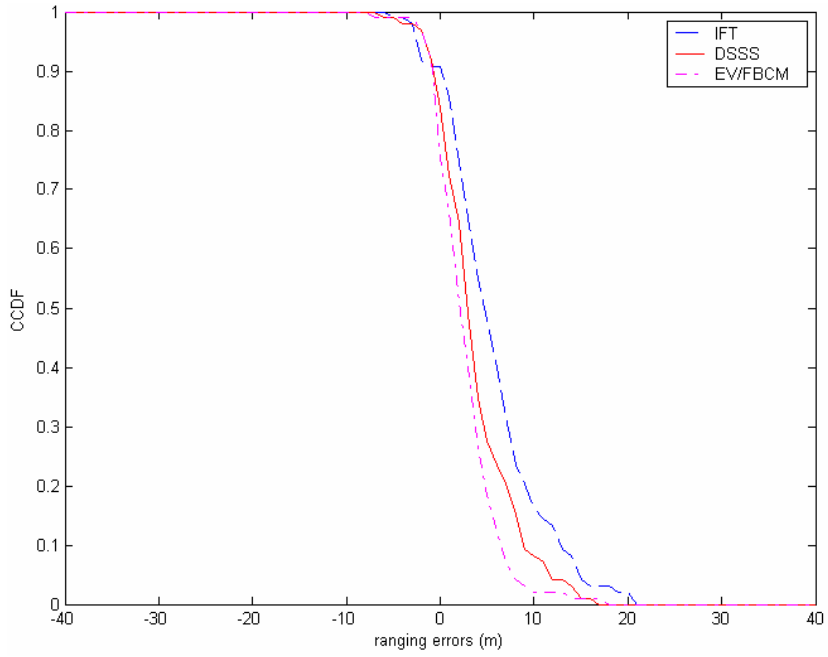

Figure A.4: CCDF Algorithm performance analysis for NDDP at 40 MHz bandwidth.

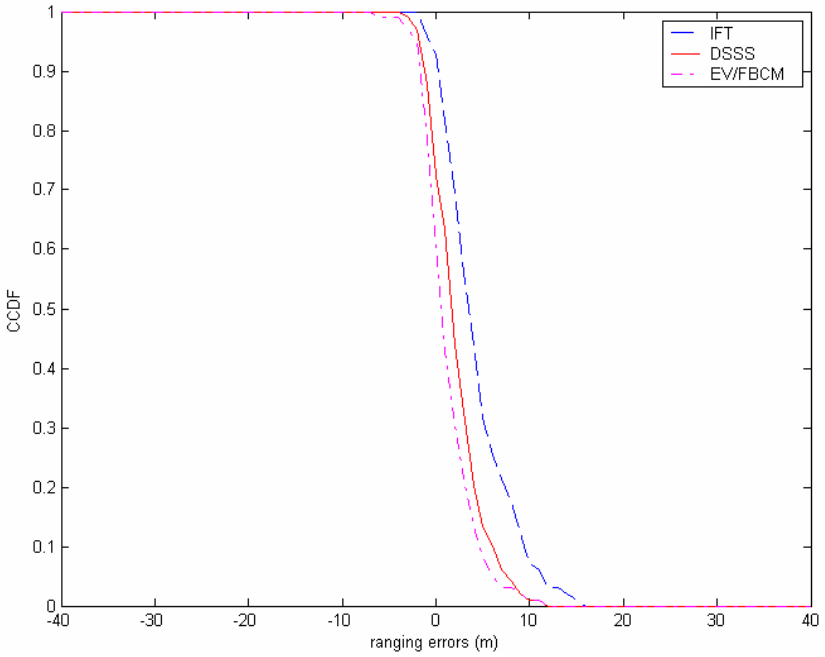

Figure A.5: CCDF Algorithm performance analysis for NDDP at 80 MHz bandwidth.

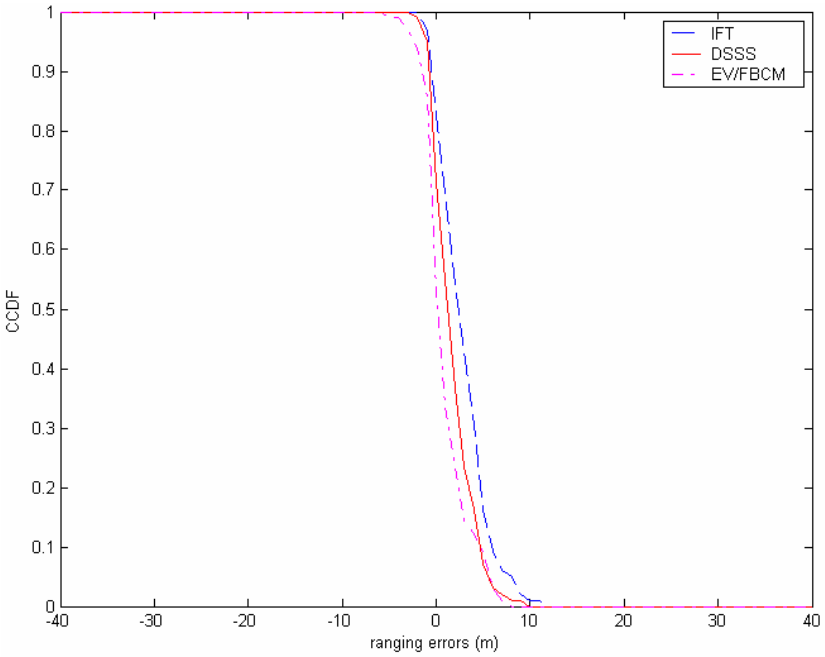

Figure A.6: CCDF Algorithm performance analysis for NDDP at 120 MHz bandwidth.

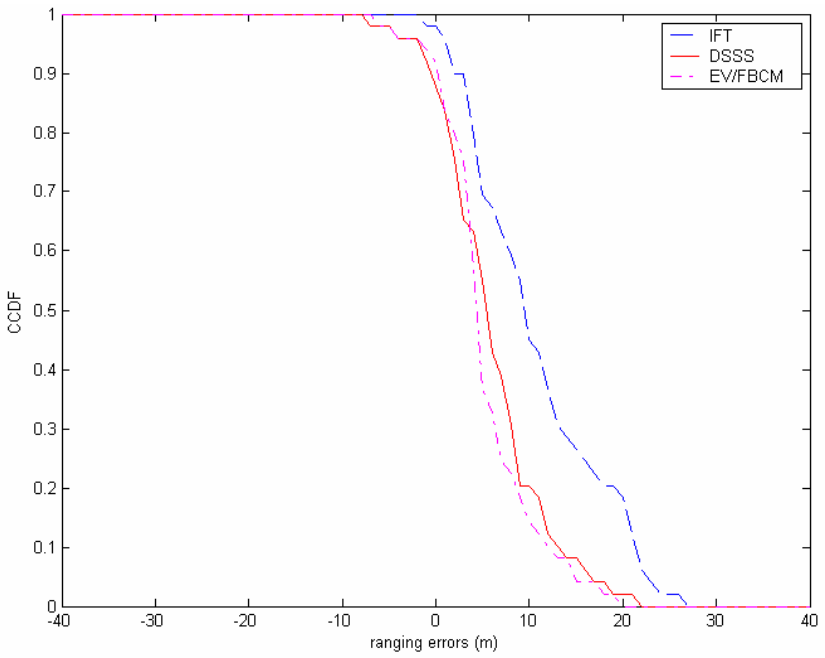

Figure A.7: CCDF Algorithm performance analysis for UDP at 40 MHz bandwidth.

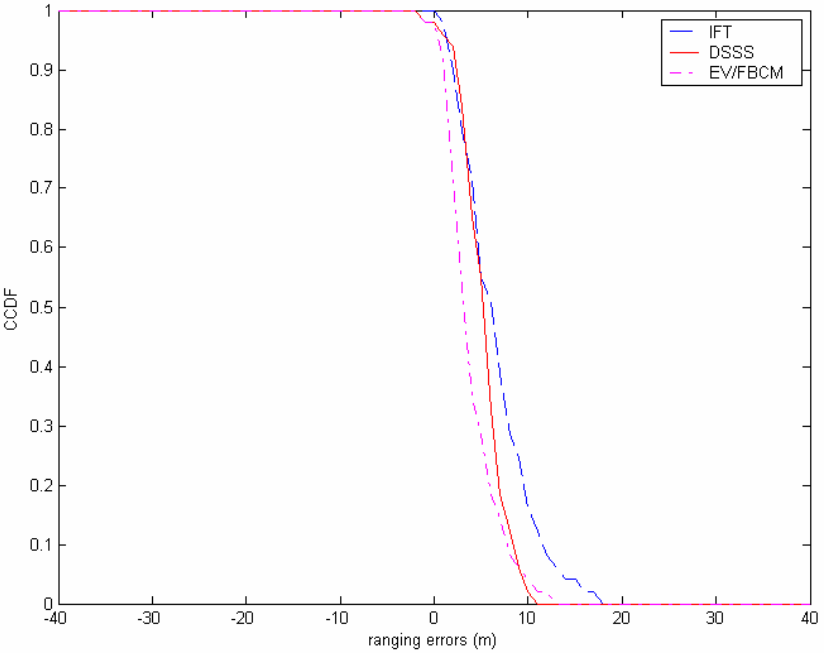

Figure A.8: CCDF Algorithm performance analysis for UDP at 80 MHz bandwidth.

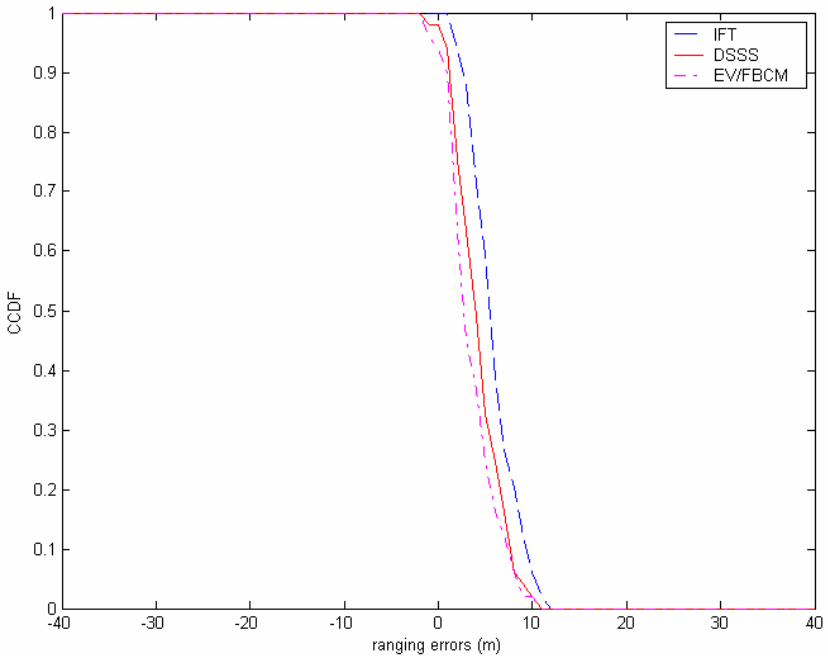

Figure A.9: CCDF Algorithm performance analysis for NDDP at 120 MHz bandwidth.

APPENDIX B Measuring and Processing Indoor Radio Channel

B.1 Introduction

The purpose of this appendix is to understand and analyze the measurement system in the frequency domain. The indoor wireless environment is characterized with multi-path effects in addition to attenuation. In order to model such environments it is important to understand the basics of channel measurements. In this appendix, a basic measurement system is described and procedures for data collection and result generation are outlined.

Calibration issues in channel measurements are also very important in obtaining reliable accurate results and this is also discussed here. There are also descriptions of the functionalities of the network analyzer and an explanation of the MATLATB code used to generate the time domain data. Finally some sample measurements that were conducted at both 1 GHz and 2.4 GHz are also provided.

B.2 Background

In analyzing wireless channels it is important to have a very good understanding of some relevant parameters. In this case the parameters that were discussed and analyzed were Time of Arrival (TOA), Path Loss and RMS delay spread. These

parameters can either be extracted from the data or calculated using a theoretical formula to obtain the desired parameter.

In the case of a simple experiment, the transmitter and receiver were positioned in Line of Sight (LOS) and the TOA is basically the time of arrival for the first path at the receiver. This can be extracted easily from either MATLAB code or the Network Analyzer. However care must be taken since the delay of the cable affects the measurements and therefore must be taken into account

In wireless channels the relationship between received power and distance has been shown in average to decrease. The relationship is given by the following expressions:

$$L_p = L_0 + 10\alpha \log_{10}(d) \qquad \text{(B.1)}$$

$$L_0 = -10 \log_{10}\left(G_t G_r \left(\frac{\lambda}{4\pi} \right)^2 \right) \qquad \text{(B.2)}$$

d = distance from transmitter to receiver

α = power gradient

Gt = Gr =1 are the transmitter and receiver gains, respectively. Most cases they are equal.

λ = c/f, where c = 3 x 10^8 m/s, f = 1 GHz or 2.4 GHz

Power gradient changes with different indoor environment. For instance open factory indoor environment have a different power gradient than indoor offices. In the

case when power gradient is around 2 then (B.1) shows that there is a 20 dB/decade of power loss. In other words the power of the transmitted signal decreases 20 dB with 10 meters of distance. Another important parameter used in channel measurements and modeling is the Root Mean Square (RMS) delay spread. With multi-path environment, the transmitted signal is reflected and refracted off of objects and at the receiver there is time spreading of the signal. This is also a good numerical measure of time dispersion. It is a better parameter when compared to excess delay spread which is the overall span of delays. RMS delay spread is the second central moment of Channel Impulse Response (CIR).

RMS delay spread is given by the following formula:

$$\tau_{rms} = \sqrt{\frac{\sum_{\kappa=1}^{N} \tau_\kappa^2 \alpha_\kappa^2}{\sum_{k=1}^{N} \alpha_\kappa^2} - \left(\frac{\sum_{k=1}^{N} \tau_\kappa \alpha_\kappa^2}{\sum_{k=1}^{N} \alpha_\kappa^2} \right)^2} \quad \text{(B.3)}$$

τ_κ is the delay time of the k^{th} tap and α_κ is the k^{th} magnitude of a tap. A tap is the individual path in the time domain. So if the time domain has three peaks then the first path has magnitude α_1 and delay τ_1; and the second has magnitude α_2 and delay τ_2. As a result the above formula provides the RMS delay spread of the CIR.

B.3 Description of the System

The overall experimental setup is composed of:

- transmitter and receiver antennas (1 GHz & 2.4 GHz)

- HP-8753B Network Analyzer with frequency range of 0.3-6000 MHz
- HP-85047A S-Parameter Test Set
- PCMCIA card & GPIB Bus
- Laptop computer

The transmitter and the receiver are connected to the S-Parameter Test Set port 1 and port 2 respectively which connect to the HP Network Analyzer as shown in Fig. 3.1. The experiment is performed by initiating a program on the laptop that asks for the required parameters such as bandwidth, start and stop time in nanoseconds and the number of samples to collect. The resulting data are composed of magnitude and phase response that gets generated in the network analyzer and collected by the laptop computer through a GPIB bus. The generated data (files) are then used for further processing using MATLAB. The antennas available are for 1GHz and 2.4GHz measurements. There are two different antennas for each frequency. These are monopole quarter-wave antenna with rectangular ground plane. The antennas attach to wooden poles that can be moved around for measuring at different locations. The HP Network Analyzer has many features and functions that could be exploited in order to process, analyze and measure data for different purposes. The main functions discussed here will have direct relevance to the experiment and any further needed functions could be easily figured out by examining the analyzer's manual.

Functions of the network analyzer include:

- Active Channels

    - Switch between channels by using the Hard Key (HK) CH1/CH2

- Auto scaling
    - Enables displaying the waveform with a best scale.
- Press on the SCALE RF HK and then select from the Soft Key (SK) menu Auto-scale
- Measuring parameters
    - Use MEAS HK to select type of measurements required
    - Use S21 for output/input measurement
- To select the format of the measurement press FORMAT HK and then select one of the SK options such as log Mag, Phase, delay, etc.
- Input
    - In the STIMILUS menu of the analyzer select START HK to choose the starting frequency/time and then use the STOP HK to select the corresponding stop frequency/time
    - From the MENU HK you can specify the required power level through the power SK

There are additional functionalities from the analyzer and they can easily be found in the user's manual.

To interface and run the program:

a. Make sure the laptop is connected to the analyzer through GPIB bus and PCMCIA card.

b. The program (Hp_meas.exe) on the laptop initiates the measurements on the analyzer

c. Before running the program make sure the analyzer has the following configured:

d. Make sure that the address is set to 17 in order to allow for synchronization between the program and the analyzer. In order to do this:

    1. In the Instrument state press the LOCAL HK
    2. From the SK options select Set Addresses
    3. Select Address 8753 SK
    4. Set it to 17

e. Once configured you can now initiate the measurements by running the following program which is on the desktop of the laptop (Hp_meas.exe)

f. The program will ask for number of samples, start and stop frequencies (f_1 & f_2) and start and stop time (t_1 & t_2).

g. The number of samples tells the program how many points you want to collect in the frequency domain. For now set the number to 400 and after going through the experiment you can easily change it to cater for your requirements

h. The range of frequency depends on your requirement and setup of the experiment. In the case you are measuring frequency response of 2.4 GHz system then the typical f_1 = 2.1 GHz & f_2 = 2.7 GHz and that would give a bandwidth of 600 MHz centered around 2.4 GHz.

i. The time duration usually starts with 0 ns and ends with 1000 ns, and that will affect the resolution for the purpose of the analyzer.

j. After deciding on the parameters then run the program by "double clicking" on the file.

k. The program will initiate the sample collection and will generate the following files:

    1. Magnitude

    2. Phase

l. Save these files for further MATLAB processing

B.4 Data Collection Procedure

In order to run the program the number of samples in the frequency domain, the bandwidth and the start and stop times are needed. The number of samples dictates to the analyzer the frequency sample spacing. This results in the following relationship: the higher the number of samples the smaller the sample spacing. This in turn has the effect on the duration of the response in the time domain. In other words, the duration of the CIR is inversely proportional to the frequency spacing. Since we are sampling in the

frequency domain then the time domain CIR will be periodic. Care must be taken in MATLAB in order to display the desired instance of the CIR. The frequency bandwidth that is used dictates to the analyzer the start and stop frequencies. They indeed have to be within the bandwidth of the antennas used. The start and stop times are used for the purpose of displaying the time domain plot on the analyzer. The frequency domain of the system is obtained by transmitting a pulse in time domain or rather a linear stepped-sweep signal in the frequency domain. The signal generated has a power of 0 dBm and therefore, there were no amplifiers or attenuators used. Obviously, in order to cover more distance it would be required to have an amplifier integrated into the system. The analyzer produces a -15 to 20 dBm swept RF signal in the range of either 900 MHz-1.1 GHz or 2.1 GHz-2.7 GHz depending on the desired range.

The following is the procedure for collecting the data:

1. After completing the analyzer setup make sure that the antennas are fixed into place.
2. Connect the transmitting antenna to Port 1 on the HP-85047A S-Parameter Test Set
3. Connect the receiving antenna to Port 2
4. Move the receiving antenna to the desired location
5. Initiate the Hp_meas.exe program located on the laptop
6. After the program initializes, it will ask for the required parameters in order to compute the frequency response

a. Enter the number of samples

b. Starting frequency

c. Stopping frequency

d. The start and stop time

e. Enter the name of the file

7. Once the measurement is completed by the analyzer then the files will be saved on the desktop of the laptop
8. The analyzer will also display the channel impulse response in the time domain on the screen.
9. Now you have just measured the frequency and phase response of the system and you have obtained the required files for further processing and analysis

B.5 Data Processing Procedure

After producing the files generated by the program then it is possible to start processing the data in order to extract and examine different parameters. The first step is to obtain the Channel Impulse Response (CIR) from the frequency and phase responses. The MATLAB code "msystem.m" contains procedure for calculating and plotting the CIR, obtaining the first path and Time of Arrival (TOA) and in addition calculating the RMS delay spread and the Path loss as well. The code uses inverse ChirpZ in order to convert the frequency domain data into time domain. The ChirpZ is a special z-transform procedure that computes the transform around a spiral contour. It makes possible

zooming into any portion of the IFFT and computes it in a certain interval with the desired number of points. It is similar to IFFT subroutine using zero padding technique. If you need any more information regarding ChirpZ the MATLAB help describes the function and its input and output parameters.

The MATLAB code has different parts and they are as follows:

1. Loading the data
    a. Load the files into MATLAB by using the infile command of file.mag and file.phs. Where file is the name of the generated phase and frequency response obtained from the measurements
    b. Convert the obtained data to linear magnitude format for further processing
2. Performing Hanning Windowing on magnitude and phase measurements
    a. Generate a Hanning sequence of the length of your linear magnitude sequence.
    b. Pass your linear magnitude values into the Hanning window
3. Computing the CIR using the Chirpz
    a. Initialize the Chirp Z parameters
    b. Compute the Chirp Z
4. Peak detection algorithm
    a. In order to establish the paths from noise

b. This depends on the level of threshold selected and must be changed for different situations

5. Plotting:
    a. Magnitude Response
    b. Phase Response
    c. CIR using Chirpz
    d. CIR with detected peaks
        i. This is the same as the CIR in c but with stem plots of the desired paths
        ii. In this case the stem plots depend on the peak detection algorithm which identifies the different paths from noise
6. Obtaining the parameters
    a. RMS delay spread can be calculated using the formula mentioned earlier. Basically, the formula gets the time delay of each path and its respective amplitude and then generates the delay spread.
    b. Average, Maximum and minimum frequency magnitude
    c. TOA of first path
    d. Magnitude of first path
    e. Total Power

f. Summation of all power components or paths results in the total power of the channel.

g. Path Loss by using (1) & (2)**.** Path loss is calculated by obtaining the received power and using the formulas.

B.6 Calibration Issues

Probably you noticed from the measured and computed results that there is something wrong. TOA at 1 meter is 162 ns? The calculated path loss doesn't compare to the theoretical? What is the problem? Like most engineering or rather scientific experiments there is always the issue of calibration. The received and processed data by MATLAB are probably right but the problem is calibration. In the case of this system there are some areas where calibration is required. For instance, did you think about the delay that the coax cable might cause? After all, the transmitting and receiving antennas are actually connected to the analyzer through coax cables. Have you considered the effect of the cable on the frequency response of your wireless channel? As it turns out, the cable has some considerable effect in altering the true response or rather characteristics of the measurements. The antennas might add some error into the results. Indeed they add some delay and/or loss to the signal. However in this procedure only calibrations which deal with the cable delay and loss will be dealt with. The following is a short procedure for identifying and removing cable effects from measurements.

The frequency response of the cable at 2.4 GHz is shown in Fig B.1. You can easily see that with such attenuation the cable calibration becomes indeed very important. In fact the cable at 2.4 GHz introduces -20 dB attenuation to the system. One way to

measure the effect of the cable on the power/path loss is to slightly alter the measurement system. In other words, a back-to-back connection is performed. This way the transmitted signal will go through the cable *only*. The same MATLAB code could be used with slight modification to compute and plot the frequency response of the system. If you intend to calibrate the path loss only then it is possible to calculate the magnitude of the peak after it passes through the cable and then this would be the cable attenuation. You can then simply remove it when applying the path loss formula. On the other hand, if you would like to remove the effect of the cable completely then you can perform some sort of channel equalization. In other words, you can multiply the magnitude response with the inverse of the cable magnitude response.

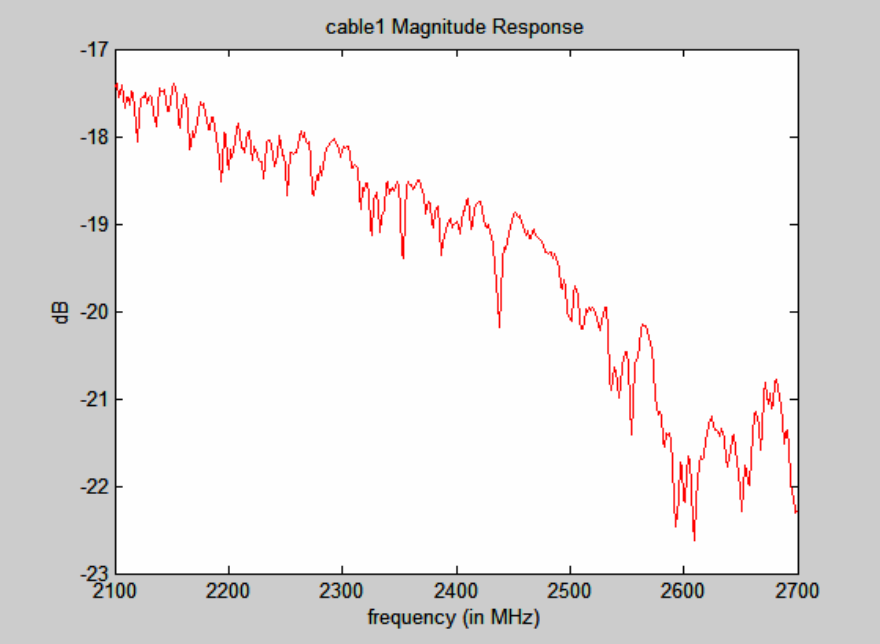

Figure B.1: Cable Magnitude frequency response

As mentioned earlier the cable also introduces a delay. Using the same "back-to-back" setup, measure the channel response but this time the signal goes through the cable only. Generate the CIR for the cable delay in MATLAB. A sample of CIR at 2.4 GHz is shown in Fig B.2. This clearly shows that the transmitted pulse in the time domain suffers delay. In this case it is around 158 ns. You can then easily add a line in MATLAB that just subtracts that delay away from the time scale so that the generated CIR and peaks are actually true and accurate.

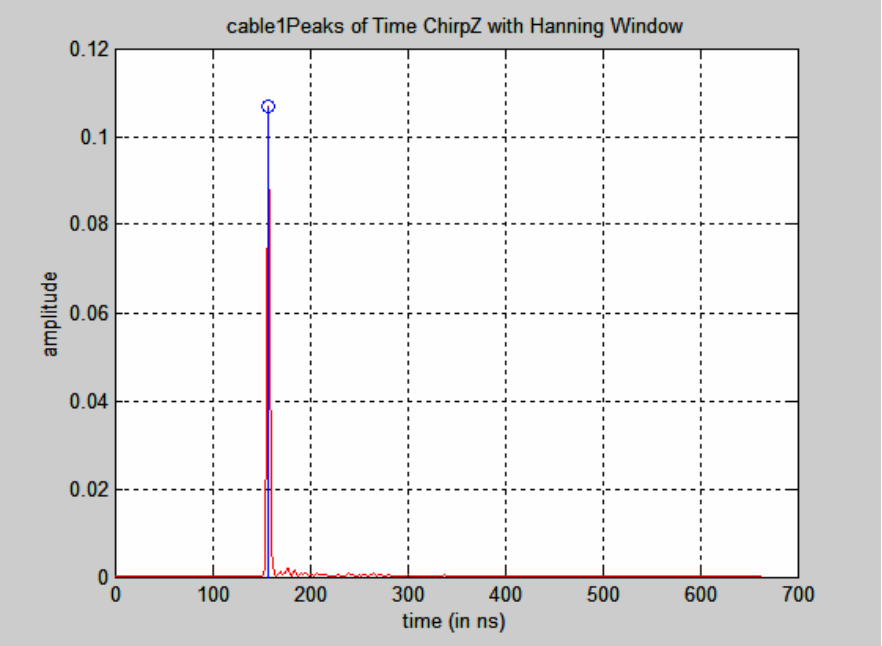

Figure B.2: Time Domain CIR

B.7 Sample Measurements

The procedure for channel measurement is usually the same for different frequency bands but sometimes some changes need to take into effect. The following is an example of channel measurements done at both 1 GHz and 2.4 GHz. The procedure

for collecting the data was shown earlier. The required parameters are also calculated according to the provided formulas.

Table B.1: Calibration Parameters

Pts	Range (MHz)	τrms (ns) MATLAB	TOA (ns) MATLAB	TOA (ns) Calibrated	Ploss (dB) MATLAB	Ploss (dB) Calibrated
400	800-1200	5.32	162.76	4.06	-44.86	-32.86
400	900-1100	6.39	162.76	4.98	-44.67	-33.6
1600	900-1100	6.56	162.76	4.45	-44.70	-33.63

As can be seen from Table B.1, the calibrated TOA at 1 meter is around 4.45 ns with a path loss of -33.63. The actual TOA should be around 3 ns, but because of additional delay from the antennas you can see that the result is off by 1.45 ns.

Again the following tables are just a sample of the results to give the reader a feel for such results and how calibration affects them.

Table B.2: 1 GHz at 10 meters

Pts	Range (MHz)	τrms (ns) MATLAB	TOA (ns) MATLAB	TOA (ns) Calibrated	Ploss (dB) MATLAB	Ploss (dB) Calibrated
400	800-1200	19.73	194.31	35.61	-56.33	-43.91
400	900-1100	27.81	194.31	36.61	-56.05	-44.98
1600	900-1100	26.42	194.26	36.56	-55.62	-44.55

Table B.3: 2.4 GHz at 1 meter

Pts	Range (MHz)	τrms (ns) MATLAB	TOA (ns) MATLAB	TOA (ns) Calibrated	Ploss (dB) MATLAB	Ploss (dB) Calibrated
400	2100-2700	6.66	162.76	4.06	-60.13	-39.78
800	2100-2700	6.25	162.13	3.43	-58.79	-38.44
400	2200-2600	7.31	161.10	3.60	-58.94	-39.52

Table B.4: 2.4 GHz at 10 meters

Pts	Range (MHz)	τrms (ns) MATLAB	TOA (ns) MATLAB	TOA (ns) Calibrated	Ploss (dB) MATLAB	Ploss (dB) Calibrated
400	2100-2700	12.18	192.65	33.95	-73.65	-53.3
800	2100-2700	11.43	192.06	33.37	-72.72	-52.37
400	2200-2600	15.75	192.65	34.95	-71.99	-52.75

In addition the following plots will show another sample of magnitude and CIR in the time domain.

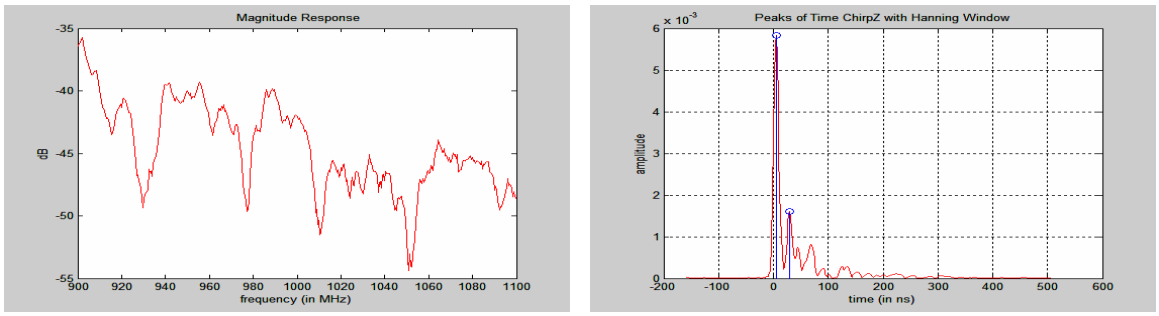

Figure B.3: Magnitude and Impulse Response of 1 GHz at 1 m

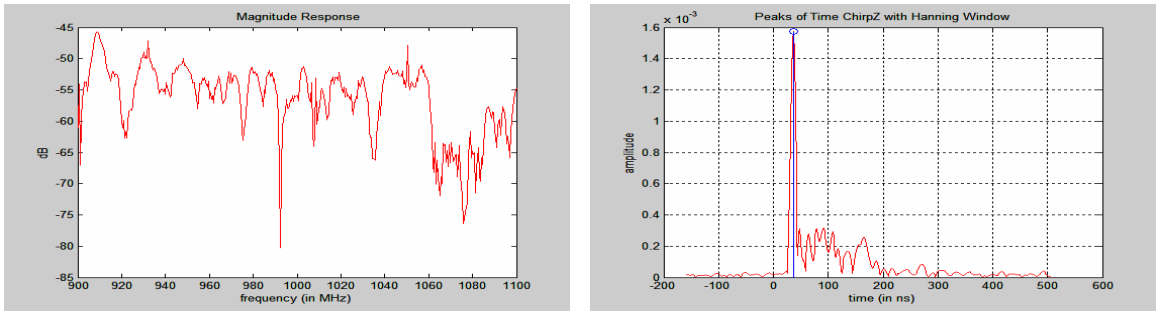

Figure B.4: Magnitude and Impulse Response of 1 GHz at 10 m

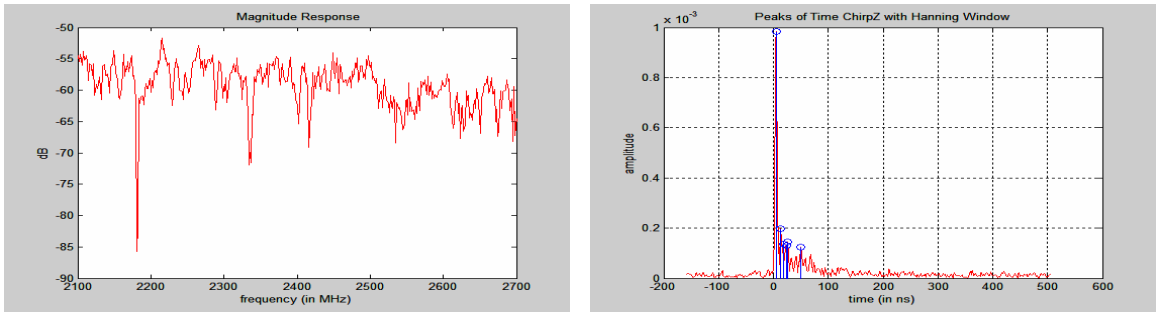

Figure B.5: Magnitude and Impulse Response of 2.4 GHz at 1 m

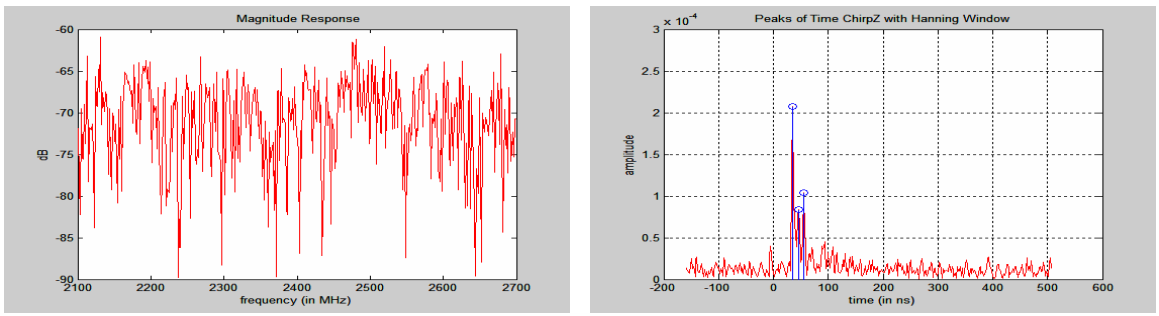

Figure B.6: Magnitude and Impulse Response of 2.4 GHz at 10 m

B.8: Summary

The measurement system introduced in this report is a basic setup without attenuators or amplifiers. There are certain important parameters to both channel modeling and indoor geo-location applications. TOA, RMS delay spread and path loss were described earlier and their measurement and calculation technique was also described. The overall system setup is composed of a network analyzer, transmitting and receiving antennas, laptop, GPIB bus and HP-85047A S-Parameter Test Set. Interfacing with the laptop through the GPIB bus was explained along with some basic functionalities of the network analyzer.

The MATLAB code used to generate the plots and calculate was also explained briefly and again the code could be used and modified to suit different measurement needs. Data collection, calculation and generation procedures were discussed from the point of view of the required parameters. Calibration issues were also discussed and it was described how to go about and account for such issues as cable path loss and delay. Finally some sample results were shown in the tables and plots.

References

[1] M. J. Meyer *et al*., "Wireless Enhanced 9-1-1 Service – Making It a Reality," *Bell Labs Tech. J.,* pp. 188-202, Autumn 1996.

[2] K. Pahlavan, P. Krishnamurthy, and J. Beneat, "Wideband Radio Propagation Modeling for Indoor Geolocation Applications," *IEEE Commun. Mag.*, vol.36, no. 4, Apr. 1998, pp. 60-65.

[3] K. Pahlavan and A. Levesque, *Wireless Information Networks*, New York: Wiley, 1995.

[4] K. Pahlavan, X. Li, and J. Makela, "Indoor geolocation sceince and technology," *IEEE Comm. Mag.*, pp. 112-118, Feb. 2002.

[5] [T. Lo, J. Litva, and H. Leung, "A new approach for estimating indoor radio propagation characteristics," *IEEE Trans. AP*, vol. 42, no. 10, Oct. 1994.

[6] G. Morrison and M. Fattouche, "Super-resolution modeling of the indoor radio propagation channel," *IEEE Trans. VT*, vol. 47, no. 2, pp. 649-657, May 1998.

[7] X. Li and K. Pahlavan, "Super-resolution TOA Estimation with diversity for indoor geolocation," *IEEE Trans. Wireless Comm.,* vol. 3, no. 1, pp. 224-234, Jan. 2004.

[8] S. J. Howard and K. Pahlavan, "Measurement and Analysis of the indoor Radio Channel in the Frequency Domain," *IEEE Trans. INSTR. Meas.,* no. 39, 1990, pp. 751-55.

[9] E. Zand, "Measurement of TOA Using Frequency Domain Techniques for Indoor Geolocation," M.S. thesis, Worcester Polytechnic Inst., 2003.

[10] J. Beneat, K. Pahlavan, and P. Krishnamurthy, "Radio channel characterization for geolocation at 1 GHz, 500 MHz, 90 MHz and 60 MHz in SUO/SAS," *Proc. IEEE MILCOM'99,* pp. 1060-1063, 1999.

[11] K. Pahlavan and P. Krishnamurthy, *Principles of Wireless Networks – A Unified Approach,* Prentice Hall, 2002.

[12] D. Manolakis, V. Ingle, and S. Kogon, *Statistical and Adaptive Signal Processing*, McGraw-Hill Co., Inc., 2000.

[13] Ekahau Indoor Positioning Software Web site, http://www.ekahau.com.

[14] N. Alsindi, X. Li, K. Pahlavan, "Performance of TOA estimation algorithms in different indoor multipath conditions", WCNC 2004, Atlanta, GA.

[15] B. Alavi and K. Pahlavan, "Modeling of the Distance Error for Indoor Geolocation", WCNC 2003.

[16] S. Howard, K. Pahlavan, "Autoregressive modeling of wide-band indoor radio propagation", *IEEE Trans.Comm.*, vol. 40, no. 9, pp. 1540-1552, May 1998.